RGB Image-Based Characterization of Dolomite Weathering for Mining Applications

Candan Alptekin

Zonguldak Bülent Ecevit University, Engineering Faculty, Department of Mining Engineering, Zonguldak-Türkiye, calptekin@beun.edu.tr; https://orcid.org/0000-0001-9209-0872

https://doi.org/10.29227/IM-2026-02-02-043

Submission date: *2026-23-07* | Review date: *2026-07-08*

Abstract

This study explores the potential of RGB image-based analysis as a predictive approach for characterizing weathering in dolomites and for guiding excavation tool optimization in mining engineering. The investigation was conducted at the Dolomite Quarry (Gebze, NW Türkiye), where two stratigraphic levels (A–B) of a representative dolomitic profile were systematically analyzed. Key indicators, such as the progression from gray tones in fresh dolomite to reddish-brown hues in weathered stages, the development of dissolution voids and microcavities, and the enrichment of clay and iron oxides, were systematically identified and evaluated. The results reveal strong and consistent correlations between RGB parameters and mechanical indices across all two stages. Fresh dolomite samples are characterized by higher UCS and SHR values, reflecting stronger resistance to mechanical excavation, while progressively weathered samples exhibit measurable decreases in strength that coincide with distinct spectral and textural transformations. These correlations confirm the capacity of RGB image analysis to differentiate intra-quarry weathering grades, and anticipate excavation challenges. The study further demonstrates that integrating RGB cameras with excavation systems can provide real-time detection of lithological and weathering transitions at the tunnel face. Such integration enables adaptive tool selection and operational adjustments that reduce cutter wear, optimize excavation efficiency, and enhance overall tunnel stability. By combining petrographic, mineralogical, and geomechanical insights with digital image analysis, this research provides an innovative, low-cost, and field-applicable methodological framework. It advances the development of intelligent excavation systems capable of responding dynamically to spatially variable rock properties, offering significant contributions to mining engineering practices in carbonate rock environments.

Keywords: *Dolomite, Weathering, RGB image analysis, Schmidt Hammer Rebound, Uniaxial Compressive Strength.*

1. Introduction

Weathering is broadly defined as the disintegration and alteration of rocks and soils through physical, chemical, and biological processes, significantly impacting the engineering properties of rock masses (Weinert 1965; Fookes et al. 1971; Irfan and Dearman 1978). Numerous studies have examined these effects across different rock types: igneous (Zhao et al. 1994; Ündül and Tuğrul 2012; Ceryan et al. 2021), metamorphic (Price and Velbel 2003; Marques et al. 2020), and sedimentary (Turkington and Paradise 2005; Matsumoto et al. 2017).

Particularly, limestones and dolomites have been extensively studied due to their widespread use. Early research linked increased porosity in carbonates to dolomitization (Murray 1960), highlighted karst-related engineering challenges (Jennings 1966), and focused on dissolution mechanisms (Blyth and Freitas 1984). Later works explored how weathering alters their mechanical behavior, strength, and durability (Tuğrul and Zarif 2000; Torabi-Kaveh et al. 2023) and their environmental roles, such as in CO_2 sequestration (Chai et al. 2024). Field studies also emphasized how climate and environmental factors influence soil and karst development (Dong et al. 2018; Küçükuysal et al. 2022), while mineral composition, grain size, and environmental exposure determine weathering profiles (Fu et al. 2023; Martínez-Martínez et al. 2023, Bilen et al. 2025). Climate-driven processes, such as chemical dissolution, shape distinctive landforms (Mareš et al. 2024), reflecting the complex interplay of lithology, climate, and geochemistry (Chang et al. 2022; Arman et al. 2019). The weathering processes affecting various rock types—and their influence on soil development, biological colonization, and engineering behavior—are schematically illustrated, as provided in Figure 1.

From an engineering perspective, weathering-controlled variations in rock properties directly influence drillability and excavation performance in both natural rock slopes and mechanized systems such as Tunnel Boring Machines (TBMs), highlighting the growing importance of image-based and photogrammetric techniques for effective rock mass characterization.

Drillability — defined as the ease or rate at which a drill bit penetrates a rock mass — is a key engineering parameter that is strongly controlled by intrinsic rock properties and weathering processes (Thuro and Spaun 1996). Numerous studies have demonstrated clear relationships between drillability and physical and mechanical rock characteristics (McFeat-Smith and Fowell 1977; Howarth et al. 1986; Kahraman 1999), with indices such as the Drilling Rate Index (DRI) widely used to link these properties to drilling performance (Yaralı and Kahraman 2011; Capik et al. 2017). Weathering-induced modifications in rock strength, porosity, and structural integrity (Fookes et al. 1971; Saunders and Fookes 1970; Ündül and Tuğrul 2012) directly influence drilling behavior. Although conventional weathering classification methods are often time-consuming, indirect approaches such as Schmidt hammer rebound and ultrasonic wave velocity measurements provide practical and efficient alternatives (Singh and Gahrooee 1989; Hack and Price 1997). Several researchers have incorporated geological features and weathering degree into drilling performance models (Bhatawdekar et al. 2019; Da Fonseca et al. 2021; Thuro 1997); however, weathering effects are still frequently underestimated or neglected in standard drillability assessments (Liang et al. 2017). These interactions between weathering and drillability are conceptually summarized in Figure 2, which combines digital drilling principles with sampling across a dolomite weathering profile to illustrate systematic changes in rock properties, including strength, porosity, and structural integrity (modified from Bilen and Sakız 2023; Fan 2025).

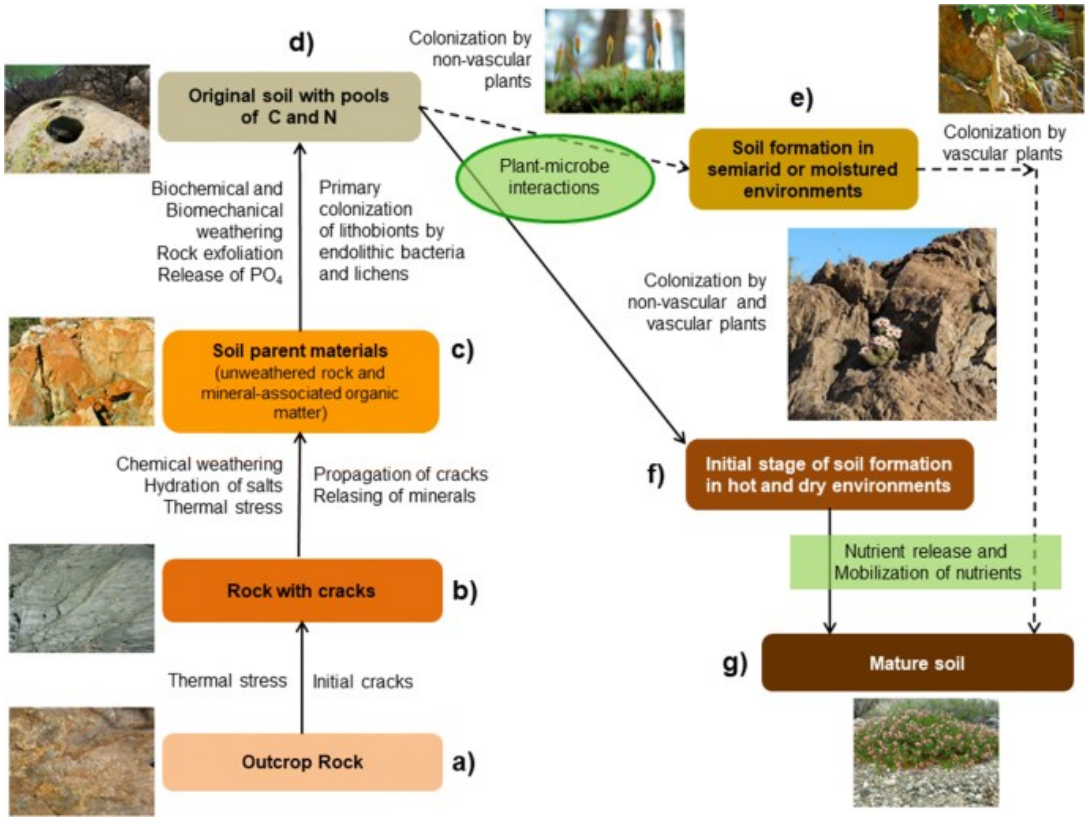

Fig. 1. Schematic representation of weathering processes across different rock types, illustrating their roles in soil formation, biological colonization, and impacts on engineering properties (Adapted from the study of Lopez and Bacillio (2020), originally modified from the study of Zhu et al. (2014)).

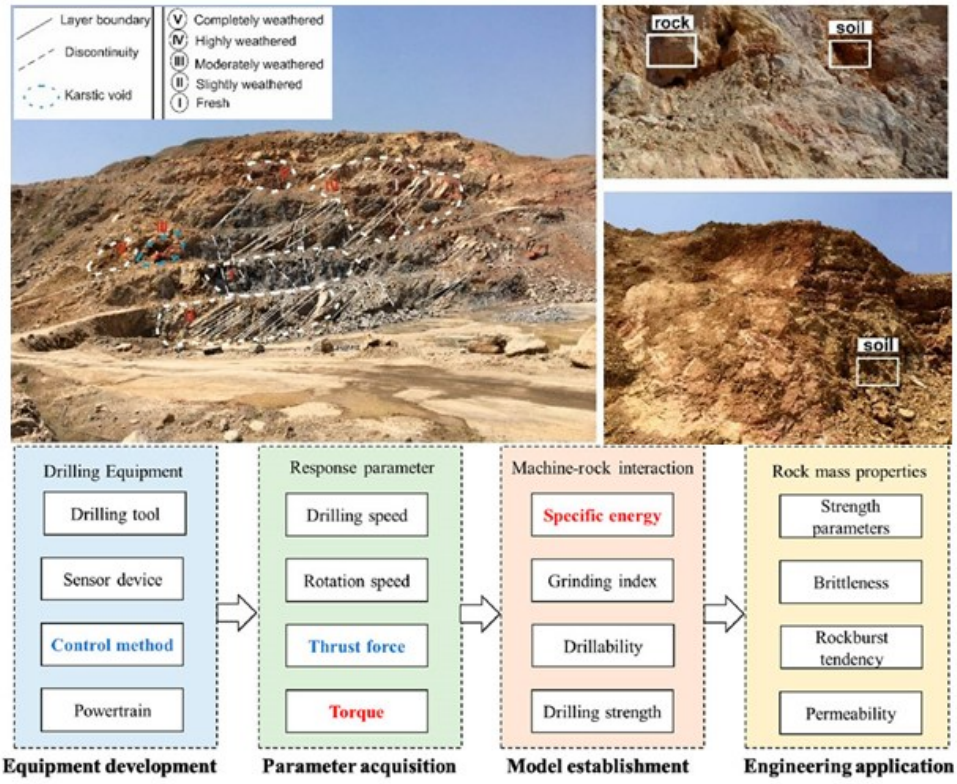

Fig. 2. Influence of weathering on rock properties affecting drillability, integrating principles of digital drilling technology and representative sampling across a dolomite weathering profile (modified from the studies of Bilen and Sakız (2023) and Fan (2025)).

Rock slopes, particularly those exposed along roads and excavations, pose significant geotechnical risks due to the inherent instability of rock masses (Sarkar et al. 2016). Weathering further reduces rock mass strength, often identifiable through visual indicators such as surface color changes (Taylor and McClennan 1985; Khan and Shamim Khan 2016). Traditional geological mapping methods can be subjective; therefore, modern techniques like image analysis and remote sensing offer more objective and reliable assessments (Azarafza et

al. 2021). Soft rocks, commonly found in weathered zones, are characterized by high fracturing, swelling, and low strength due to advanced degrees of weathering (Terzaghi and Peck 1967; Rocha 1975; Dobereiner 1984; Johnston 1993; Gonzalez de Vallejo et al. 2002; Kanji 2014; Zhu 1985). These rocks are typically defined by uniaxial compressive strength (UCS) values below 12.5–25 MPa (Bieniawski 1984; Barla et al. 1990; Russo 1994; Kanji 2014). In tropical climates, chemical weathering is especially aggressive, accelerating the decomposition of rock material (Puente et al. 2006; Komoo 1995; Alavi Nezhad Khalil Abad et al. 2014; Ng et al. 2001; Chiu and Ng 2014). This degradation has major implications for engineering works involving foundations, slopes, embankments, and tunnels, where insufficient consideration of weathered conditions can result in instability, erosion, and drainage problems (Abad et al. 2015). These relationships between weathering, slope stability, and soft rock behavior—based on field and laboratory assessments of sandstone, mudstone, and limestone at multiple road cuts (Ersöz and Topal, 2018).

Tunnel Boring Machine (TBM) performance is highly sensitive to the geomechanical conditions of the rock mass, with adverse geological factors such as rockburst, mixed ground, and high-stress zones significantly influencing safety and efficiency (Khetwal et al. 2020; Li et al. 2021; Zhao et al. 2018). Traditionally, rock mass characterization has relied on laboratory tests like uniaxial compressive strength or point load tests (Chen et al. 2021; Xie et al. 2021), as well as forward geological prospecting methods (van Eldert et al. 2020; Li et al. 2017). While these approaches are useful, they are time-consuming, costly, and fail to provide real-time, continuous feedback during excavation (Wu et al. 2021; Zhang et al. 2019). To overcome these limitations, recent studies have highlighted the potential of analyzing the excavated material—an immediate outcome of the rock–machine interaction—as a proxy for rock mass conditions (Liu et al. 2021; Zhang et al. 2021). Indeed, parameters such as fragment size, shape, and distribution have been shown to correlate with boring efficiency, fragmentation behavior, and even tunnel stability (Farrokh and Rostami, 2008; Tuncdemir et al. 2008; Heydari et al. 2019).

Advances in digital image processing (DIP) and RGB image analysis provide an efficient and field-applicable method for extracting detailed information from excavated material (Huang et al. 2021; Bagheri et al. 2015; Xie et al. 2020). By converting RGB images of the muck into binary or quantified datasets, it becomes possible to calculate particle size, morphology, and distribution automatically (Zhang et al., 2021; Amankwah and Aldrich, 2011). These methods allow for real-time monitoring of the excavation front by installing cameras on the TBM conveyor system, thus enabling a continuous perception of the rock–machine interaction without halting operations. Such integration of RGB-based analysis not only enhances the predictive power of TBM performance models but also supports intelligent, adaptive decision-making to optimize cutterhead wear, penetration rate, and overall excavation efficiency (Gong et al., 2021; Wu et al., 2021). A conceptual overview of the RGB-based real-time feedback system and its integration with underground sensing technologies for TBM performance optimization is illustrated in Figure 3 (adapted from the study of Zhu et al., 2025).

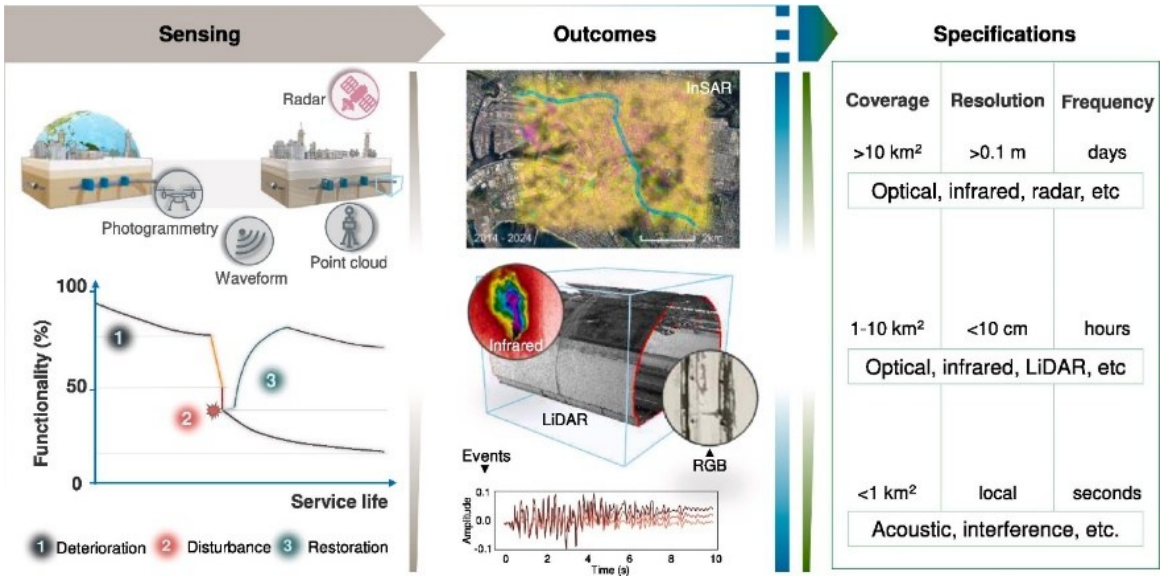

Fig. 3. RGB image-based analysis and underground sensing technologies for real-time TBM monitoring and performance optimization (adapted from the study of Zhu et al. 2025).

Photogrammetry and UAVs enable high-resolution imaging of outcrops and rapid weathering assessments over large areas (Leu and Chang 2005). For example, the JudGeo tool classifies weathering zones based on CIELAB color parameters, which are more reliable than RGB values. Nevertheless, since surface weathering does not always reflect subsurface conditions, validation through mechanical tests such as the UCS-Schmidt hammer remains essential (Azarafza et al. 2021). Techniques like spectrophotometry (Luo et al. 2020), laser scanning (Ismail et al. 2020), and colorimetric analysis (Sousa and Gonçalves 2012) have shown promise, but challenges such as lighting variability and field conditions persist (Tating et al. 2013; Alavi Nezhad Khalil Abad et al. 2015, 2016).

Weathering also causes gradual color changes in rocks, traditionally assessed through systems like Munsell (Munsell and Nickerson 1915; Cleland 1921) and more recently using digital color spaces like CIELAB (Connolly and Fleiss 1997; Service 2013). As surface layers peel away, revealing fresher material, significant and measurable color differences emerge (Gökay 2018). Studies on color changes due to iron oxide (Nagano and Nakashima 1989) or oxidation and biological growth (Grossi et al. 2015) have further demonstrated the usefulness of color as an indicator of weathering. The integration of RGB color analysis with geological mapping to visualize these weathering patterns and crack distributions is illustrated in Figure 4 (adapted from Yusoff et al., 2021).

In mining, maintaining ore quality is crucial for economic viability. Traditional monitoring methods, based on manual sampling and laboratory analysis, are time-consuming and labor-intensive. Image-based sensor technologies offer fast, contactless, real-time quality estimation (Singh & Rao 2005; Malamas et al. 2003).

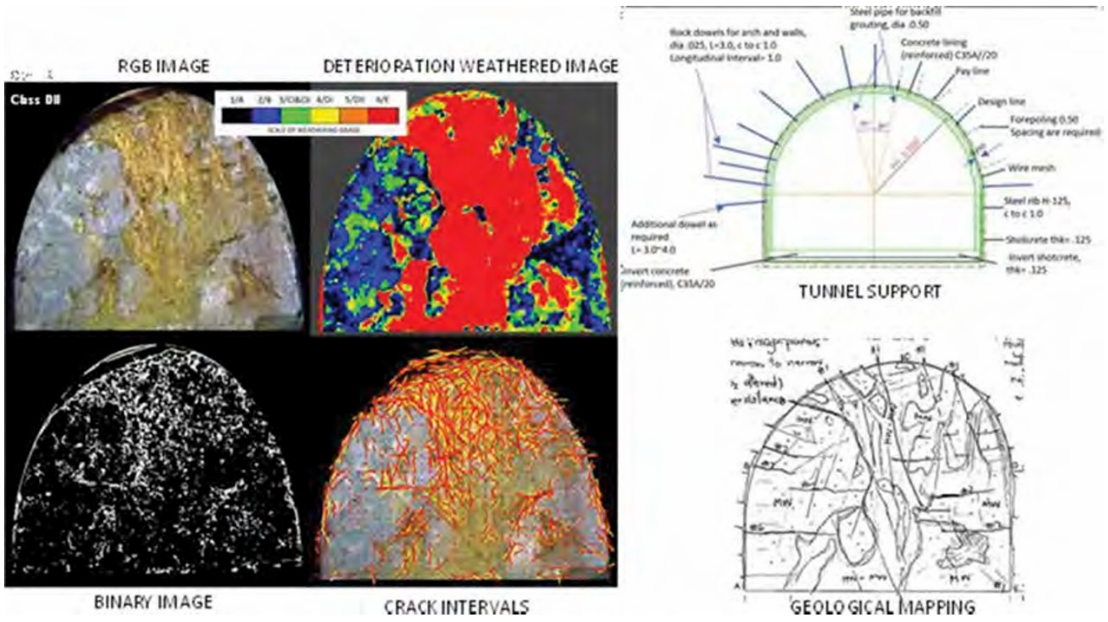

Fig. 4. Visual representation of weathering zones and surface crack patterns identified through RGB color analysis and geological mapping (adapted from Yusoff et al. 2021).

Numerous studies have demonstrated the applicability of image analysis to estimate particle size, mineral composition, and grindability (Oestreich et al. 1995; Petruck and Lastra 1993; Shafarenko et al. 1997; Casali et al. 2000; Petersen et al. 1998; Henley 1983; Jones and Horton 1979; Lin et al. 1993), although direct prediction of ore grade remains underexplored. Visual judgment is already a common practice in mines, as operators differentiate ore from waste based on appearance — a practice that image-based systems aim to standardize and automate. Similarly, carbonate rocks (limestone and dolomite), widely used in civil engineering, are evaluated through their uniaxial compressive strength (UCS), a key indicator of load-bearing capacity. Textural classifications (Dunham 1962; Embry and Klovan 1971) help predict mechanical behavior, as texture and mineralogy influence porosity and strength. In northwestern Türkiye, limestone and dolomite quarrying is widespread, and accurate UCS assessment is crucial (Felekoglu 2007; Rajabi et al. 2017; Bilen 2021). Since UCS tests are costly and slow, digital image analysis of thin-section images, combined with color metrics (RGB, HSV), provides a promising alternative.

Studies show that weathering-induced color variations correlate with strength properties (Toś 2016; dos Anjos et al. 2021; Zhao et al. 2021; Tembely et al. 2021). By applying machine learning and petrographic quantification, researchers have demonstrated that microscopic features captured in high-resolution images can predict macro-scale engineering properties. For instance, convolutional neural networks (dos Anjos et al. 2021), CT imaging (Zhao et al. 2021), and near-infrared enhanced classification (Toś 2016) have all contributed to this evolving field. These approaches suggest that image-based, non-invasive methods can effectively link microscopic petrographic characteristics with engineering performance, offering practical solutions for strength and weathering assessments of carbonate rocks. Integrating RGB and RGB+NIR imaging, machine learning, and petrographic texture analysis, these image-based methods enable real-time ore quality monitoring, automated differentiation, and non-invasive prediction of carbonate rock strength and weathering effects — as conceptually illustrated in Figure 5 (adapted from Toś, 2016).

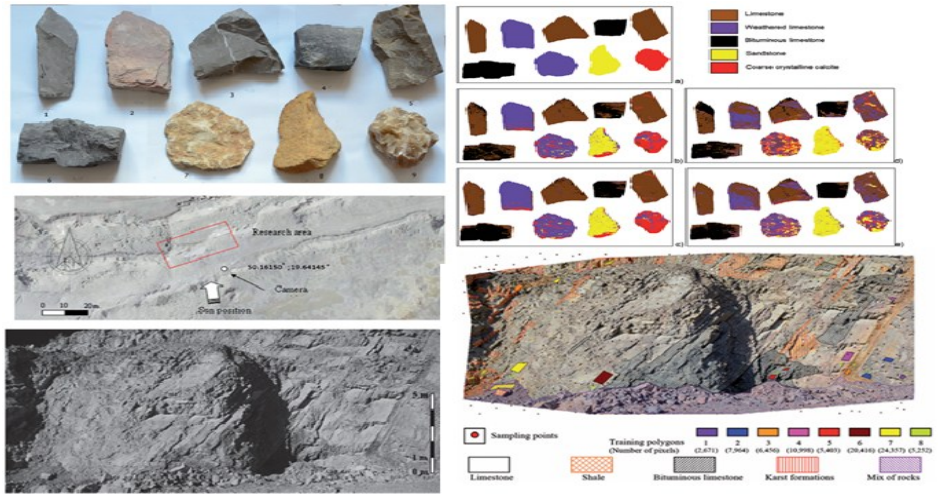

Fig. 5. Image-based analysis methods for assessing ore quality and rock strength, combining RGB and RGB+NIR classification of carbonate rock types, quarry wall mapping, and petrographic texture evaluation (adapted from Toś, 2016).

Building on this body of research, the present study aims to demonstrate the potential of RGB image-based weathering degree assessment of dolomite thin sections as a predictive tool for optimizing excavation equipment in tunnel engineering. By analyzing thin-section images from quarries in the Gebze region, the study seeks to establish links between microstructural color variations and weathering-induced

mechanical changes. The ultimate objective is to develop an RGB-based, low-cost, real-time model that can guide the selection and adaptation of excavation tools in response to varying rock strength and weathering profiles encountered during tunneling operations.

2. Geology of the Study Area

Samples for this study were collected from quarries located in the Gebze region (NW Turkey) (Figure 6). The dolomite used in this study were collected from the Lower Triassic Ballıkaya Formation. The Ballıkaya Formation has been previously described and studied by researchers, such as Erguvanlı (1949), Altınlı (1968), and Gedik et al. (2005) (Figure 7).

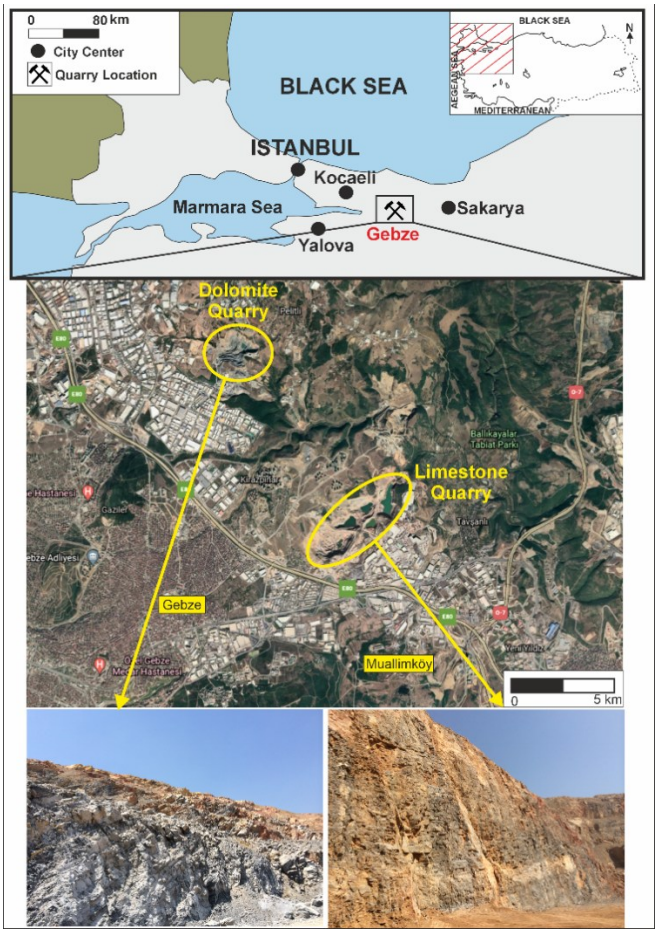

Fig. 6. Location map of the study area and general view of limestones and dolomites observed in the study area (adapted from the study of Bilen et al. 2025).

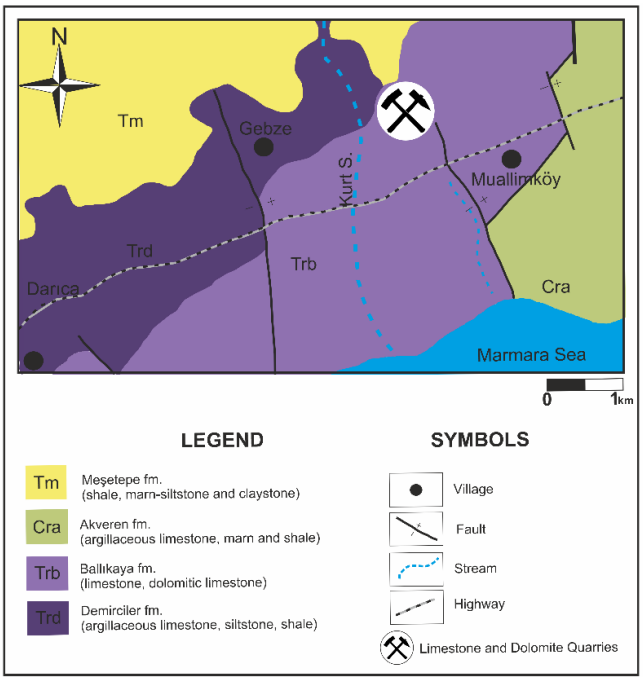

Fig. 7. Geological map of the study area and its surroundings (adapted from Gedik et al. 2005, Bilen et al. 2025)

The Ballıkaya Formation consists of limestone, dolomite and dolomitic limestone. In relatively fresh sections, the observed limestones exhibit gray and light–dark gray colors, whereas in weathered sections, they generally appear yellowish brown (Figure 6). The limestones are mostly sparitic and fossiliferous. They also contain calcite veins with thin- to medium-sized crystalline structures. The thicknesses of the limestone layers vary from thin to medium at the base and from thick to very thick in the upper sections of the formation.

Dolomites are generally bluish gray and dark gray in color (Figure 6). Similarly, in weathered sections, the dolomites also display yellowish brown colors. The dolomites in the Ballıkaya Formation exhibit a semieuhedral mosaic texture, which is characterized by dolomite and calcite crystals. Conchoidal (seashell-shaped) fractures and nodular (silica–chert) structures are the dominant features observed in dolomites.

The limestone- dolomite quarry in Gebze region, demonstrates significant potential for high-quality aggregate production. The Ballıkaya Formation, a Triassic-aged unit extensively studied for its aggregate potential, dominates this area. It comprises dense, fine-to-medium-grained limestones with dolomitic intercalations and is often characterized by karstic cavities filled with red clay and silt. Stratigraphically, the formation is noted for its dolomitic limestone, micritic, and sparitic compositions, which influence its suitability for specific engineering applications. The region's limestone demonstrates high calcite content, providing excellent adherence to cement in concrete applications. Geomechanical testing reveals uniaxial compressive strength values within acceptable limits for construction aggregates, supported by its specific gravity and low water absorption rates. The results indicate that Gebze limestones meet standard requirements for producing lightweight concrete aggregates, road base materials, and stabilization fillers. Further tests, such as Los Angeles abrasion, ensure durability under mechanical stress, confirming its versatility for engineering purposes (Dursun 2004).

The dolomite quarries in the Gebze region offer opportunities for construction materials, particularly in road and infrastructure projects. Dolomitic rocks in the Ballıkaya Formation exhibit distinct geotechnical behavior due to their magnesium-rich composition and susceptibility to weathering. Field studies and laboratory experiments show increased porosity and reduced density in weathered zones, impacting mechanical performance metrics such as uniaxial compressive strength and water absorption. Mineralogical studies reveal that dolomite from the Gebze area contains varying proportions of calcite and dolomite, influencing its durability and application potential. Advanced analyses highlight the impact of structural discontinuities caused by tectonic activity, which leads to fracture development and facilitates weathering processes. Geological investigations segment the quarries into zones with distinct material quality, optimizing resource extraction. Tests such as freeze-thaw resistance, impact value, and crushing value underscore the aggregates' resilience in dynamic environmental conditions. These evaluations confirm the suitability of dolomite as an essential raw material for base layers in road construction, as well as its potential for stabilized fill and ballast applications (Erkol and Aydındağ 2012, Akyıldırım and Karakaş 2021, Bilen et al. 2025).

3. Material and Method

Dolomite samples were collected from an open pit quarry. Dolomite quarry under investigation are located in Gebze/Kocaeli Turkey. Briefly explaining the geology, the region is in Hereke formation and it has many quarries operated at this site. The location map of the study area is provided in Figure 1. In Figure 2, geological map of the study area (adapted from the study of Gedik et al. 2005) was provided. General view of the limestone-dolomite quarries under investigation can be seen in Figure 8 (Bilen 2021).

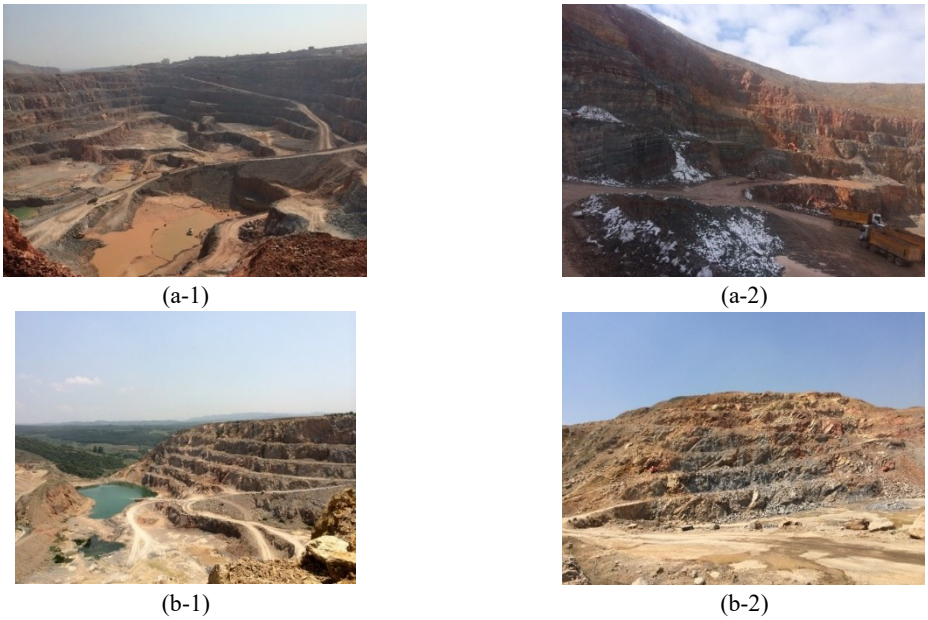

(a-1) (a-2)

(b-1) (b-2)

Fig. 8. General view of the dolomite quarries under investigation, refer to (a-1) and (a-2) for limestone & (b-1) and (b-2) for dolomite (Bilen 2021).

In the beginning of the sample collection, each level of the profile were divided into 45 interval, i.e. each interval is 1 m length and that abovementioned profile, i.e. dolomitic profile has 4 levels. The aforementioned sampling locations were considered not only as the locations where SHR values were obtained from but also 5 m intervals were chosen as the sampling location for mechanical tests (UCS) along with the petrographic analyses (thin section analyses) tests. See Figure 9 in order to better represent sampling in situ, i.e. red circles. Initial collected samples are in the form of blocks (Bilen 2021).

3.1. SHR Tests

Schmidt Hammer Rebound tests were carried out in-situ and standard method i.e. ASTM Stand. (D 5873-00) (2001) was taken into consideration. A total of approximately 518 points were considered in terms of SHR tests. In order to carry out in-situ SHR testing, initially

each level (4 levels for each profile; one profile in limestone, two profile in dolomite) was marked along 1 m intervals, i.e. 45 points for each level, a total of 540 points were marked. Horizontal distance for each point was 1 m for each interval and the vertical distance of each point (distance from the bottom of the level) is roughly 1.5 m. During the time of this study, levels (4 levels in limestone and 8 levels in dolomite) under operation have had a variety of height, i.e. 4-10 m. Vertical distance of the SHR tested points were chosen according to their availability of a human height (See Figure 9 for details). This method was originally employed in the study of Bilen (2021), and only the dolomitic profile was under investigation in the context of this study. (Bilen 2021). Same methodology in terms of SHR tests, mechanical tests (UCS) which is originally investigated by Bilen (2021) in order to evaluate SHR-UCS-HGI interrelationships is also taken into consideration in this context of the current study.

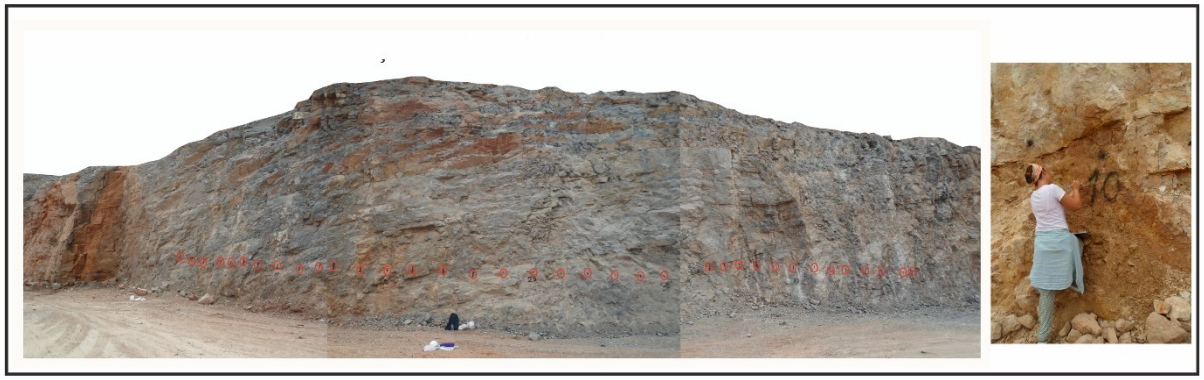

Fig. 9. Marked points in a level (red circles, at the bottom) and SHR testing in-situ (Bilen 2021).

SHR tests were the initial step of the performed in-situ work. In the order of SHR tests, a number of 10 measurements with Schmidt Hammer was considered. Abovementioned 10 measurements with Schmidt Hammer were performed nearby the point under interest depending on the availability (surface roughness and weathering considered in this case). Average of SHR measurements (10 measurements) was noted down for that specific marked point. Due to residual soil structure of some points or lack of availability in general, SHR tests were not performed on some points marked. That is why, a total of 518 points were considered, i.e. 22 points were disregarded (Bilen 2021).

3.2. Sample Preparation & Mechanical Tests

Samples are initially in the form of block samples as it was expressed earlier. Block samples were collected from the sampling area (nearby the sampling point) and this sampling area was chosen accordingly ±2 m (roughly) nearby the numbered sections of the levels. Depending on the availability, different number of block samples (at least one) were collected from each sampling point. A total of 36 block samples were collected from the quarry under investigation. Associated laboratory work was carried out on the block samples and firstly cylindrical core samples were prepared for UCS testing. A total of 175 cylindrical specimen were prepared. Cylindrical core samples were prepared by employing laboratory drilling and sawing machines. A graphical representation of block samples (collected) and prepared cylindrical core samples were provided in Figure 10. Mechanical tests were carried out on the core samples prepared from the each representative samples collected from the quarries. In terms of mechanical tests, only UCS was considered in this study. The standard method of ISRM (2007) was considered in terms of UCS tests.

Fig. 10. Representation of cylindrical core samples preparation from the collected block samples.

3.3. Petrographic Characteristics-Thin Section Analyses

The petrographic characteristics of the studied rocks, including the relative existence of mineral grains and the matrix, were determined via thin section analyses under a polarized petrographic microscope. At least 6 thin section images were obtained from the each sample, 2 of which is classified as fresh samples, and 4 of which is intended to be the weathered classified ones. Since each thin sections images were carefully analyzed and purposely number of 4 images were taken to represent different degrees of weathering within each zone. This approach allowed the researchers to examine changes in the mineralogical composition, texture, and fabric of rocks as they transition from

fresh to completely weathered states. However, the preparation of thin sections from residual soil (WVI) was not possible (Bilen et al. 2025).

As part of the laboratory studies, thin sections prepared to determine the petrographic properties of dolomite samples belonging to different weathering classes were initially produced at the Thin Section Preparation Laboratory of Pamukkale University, Earthquake Research Center. In total, 191 thin sections, 51 of which for dolomitic profile (See Figure 18), were prepared to identify the petrographic features of the samples, characterize internal weathering stages, and observe weathering classes that are not visible in the field at a microscale. Detailed examinations of these thin sections were conducted and photographed using a LEICA DM 750 P polarized microscope at the Mineralogy-Petrography Division, Department of Geological Engineering, Istanbul University-Cerrahpaşa (Figure 11). Through these polarized microscope analyses, the types, mineral compositions, and petrographic weathering classifications of the dolomite samples were determined (Bilen 2020).

(a) (b)

Fig. 11. Some of the thin sections evaluated in the context of this study (a) Examination and photography of thin sections under a polarizing microscope (b). Note that a total of 216 thin section images investigated in the context of this research (Dolomite Quarry).

In terms of thin section analysis, firstly some thin section sampling was carried out from the collected block samples. Prepared thin section samples for Dolomite, Stage A is provided in Table 1. For each level of the Dolomite Quarry (P2L1 (Profile 2-Level 1), P2L2, P2L3, and P2L4), 54 thin section images were analyzed, resulting in a total of 216 images examined across the two stages.

3.4. Image Processing and RGB-HSV Analyses

In order to process the thin section images taken, an online software (online tool for image processing) was employed. This abovementioned online tool is open source and it is actually referred as "Image Color Summarizer" by Martin Krzywinski. The following link for this online tool is as "https://mk.bcgsc.ca/colorsummarizer/?analyze". The abovementioned online program analyzes the images and provide a result page including RGB and HSV (min, max and average) (See Figure 12).

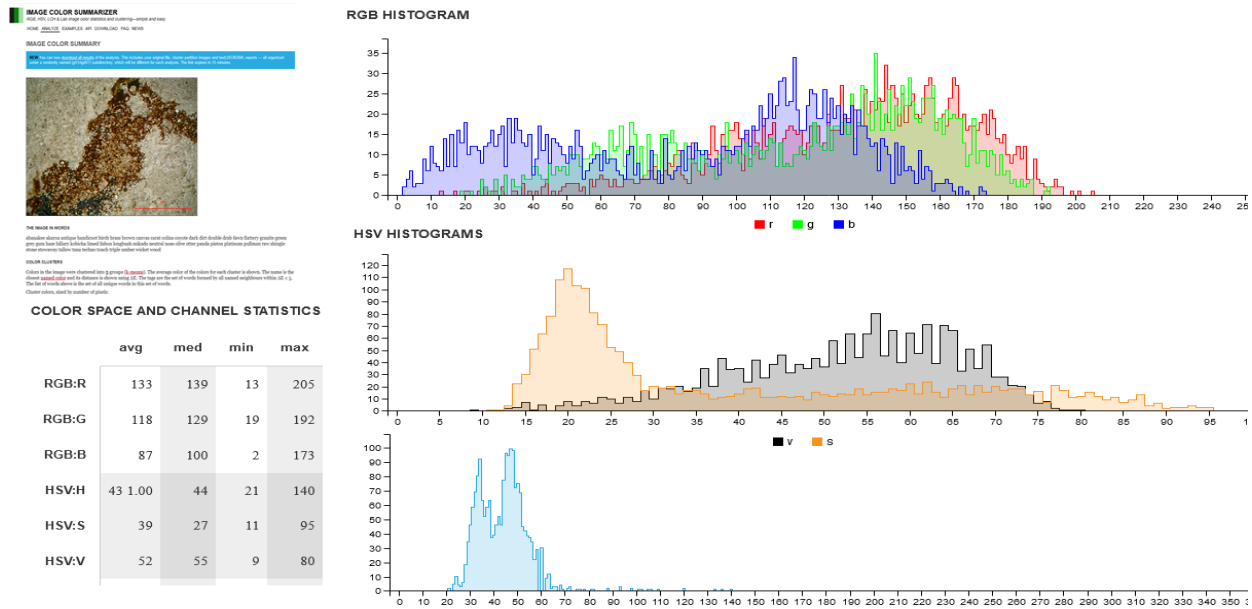

Fig. 12. A representation of image analysis result obtained from an online tool by Martin Krzywinski (URL-1, 2025) ("https://mk.bcgsc.ca/colorsummarizer/?analyze").

3.*5. Schmidt Hammer Rebound Value Measurements of Dolomite Stage A Samples*

Based on the study carried out in the context of Bilen (2021), Schmidt Hammer Rebound (SHR) values and Uniaxial Compressive Strength (UCS) values were provided (See Table 1, left column). In this context, thin section images not only from fresh surfaces but also from weathered surfaces obtained in the order of corresponding each UCS sampling are provided in Table 1 (See images on the right column). In addition to these thin section images, R, G, B and H, S, V values of these corresponding images (on the right column) are tabulated in Table 1 (See Table 1, middle column).

Tab. 1. SHR values & UCS values and thin section images of Dolomite Stage A, P2L1.

SHR and USC Results

Schmidt Point	Average SHR value	UCS Value
P2L1-1	33.6	
P2L1-2	21	
P2L1-3	32.8	
P2L1-4	34.4	
P2L1-5	27.6	30.59
P2L1-6	20.8	
P2L1-7	25.2	
P2L1-8	31.8	
P2L1-9	32	
P2L1-10	32.8	43.54
P2L1-11	22.4	
P2L1-12	20.2	
P2L1-13	40.4	
P2L1-14	23	
P2L1-15	35.6	78.10
P2L1-16	24.6	
P2L1-17	23.6	
P2L1-18	21.6	
P2L1-19	21.2	
P2L1-20	28	33.67
P2L1-21	26	
P2L1-22	29	
P2L1-23	31.8	
P2L1-24	23.8	
P2L1-25	35.2	67.91
P2L1-26	35.6	
P2L1-27	38.2	
P2L1-28	37	
P2L1-29	33	
P2L1-30	42.8	127.13
P2L1-31	37.8	
P2L1-32	37	
P2L1-33	30	
P2L1-34	36.6	
P2L1-35	34.8	68.16
P2L1-36	26	
P2L1-37	38	
P2L1-38	31	
P2L1-39	28.8	
P2L1-40	31.2	66.68
P2L1-41	25.2	
P2L1-42	33.4	
P2L1-43	31.8	
P2L1-44	40	
P2L1-45	27.6	36.71

le Representation resh Surfaces	Sample Represent Weathering Surf
f-1	w-1
f-2	w-3

Image Analysis of Thin Sections

Fresh Surfaces (f-1)

P2	R	G	B	H	S	V
L1-5	66	65	51	57	23	26
L1-10	69	68	55	56	22	27
L1-15	78	76	63	54	21	31
L1-20	66	65	53	56	22	26
L1-25	76	74	60	53	22	30
L1-30	85	80	63	49	26	33
L1-35	78	75	61	52	22	31
L1-40	77	75	60	54	22	30
L1-45	67	66	53	56	21	27

Fresh Surfaces (f-2)

P2	R	G	B	H	S	V
L1-5	65	64	50	56	23	26
L1-10	68	67	54	55	22	27
L1-15	80	76	62	47	23	31
L1-20	68	67	54	56	21	27
L1-25	80	77	63	52	22	31
L1-30	93	88	72	45	23	37
L1-35	78	75	61	48	22	31
L1-40	75	73	60	54	22	30
L1-45	67	66	52	56	23	26

Weathered Surfaces (w-1)

P2	R	G	B	H	S	V
L1-5	66	66	54	59	20	26
L1-10	74	72	58	53	22	29
L1-15	76	74	62	56	19	30
L1-20	70	68	54	54	23	28
L1-25	81	79	66	54	19	32
L1-30	134	121	90	45	41	52
L1-35	81	78	63	50	23	32
L1-40	76	75	61	54	20	30
L1-45	70	69	55	55	22	28

Weathered Surfaces (w-2)

P2	R	G	B	H	S	V
L1-5	62	61	48	58	25	25
L1-10	68	67	54	56	23	27
L1-15	86	83	71	49	18	34
L1-20	65	65	52	63	22	26
L1-25	77	75	60	54	23	30
L1-30	126	123	110	54	22	50
L1-35	78	76	62	51	22	31
L1-40	76	74	61	53	21	30
L1-45	66	65	53	61	21	26

Weathered Surfaces (w-3)

P2	R	G	B	H	S	V
L1-5	63	63	50	59	22	25
L1-10	70	70	58	61	18	28
L1-15	83	80	66	52	21	33
L1-20	64	64	51	58	22	25
L1-25	82	79	66	50	19	32
L1-30	112	108	94	48	16	44
L1-35	78	75	59	51	24	31
L1-40	76	73	58	52	24	30
L1-45	68	67	55	57	21	27

Weathered Surfaces (w-4)

P2	R	G	B	H	S	V
L1-5	59	62	50	89	35	25
L1-10	75	72	56	54	27	30
L1-15	85	80	64	47	27	34
L1-20	64	63	51	59	22	25
L1-25	83	78	63	46	25	33
L1-30	112	104	80	45	31	44
L1-35	83	79	64	48	24	33
L1-40	80	78	62	53	26	32
L1-45	71	68	52	53	28	28

Dolomite Stage A (Level-1) Samples

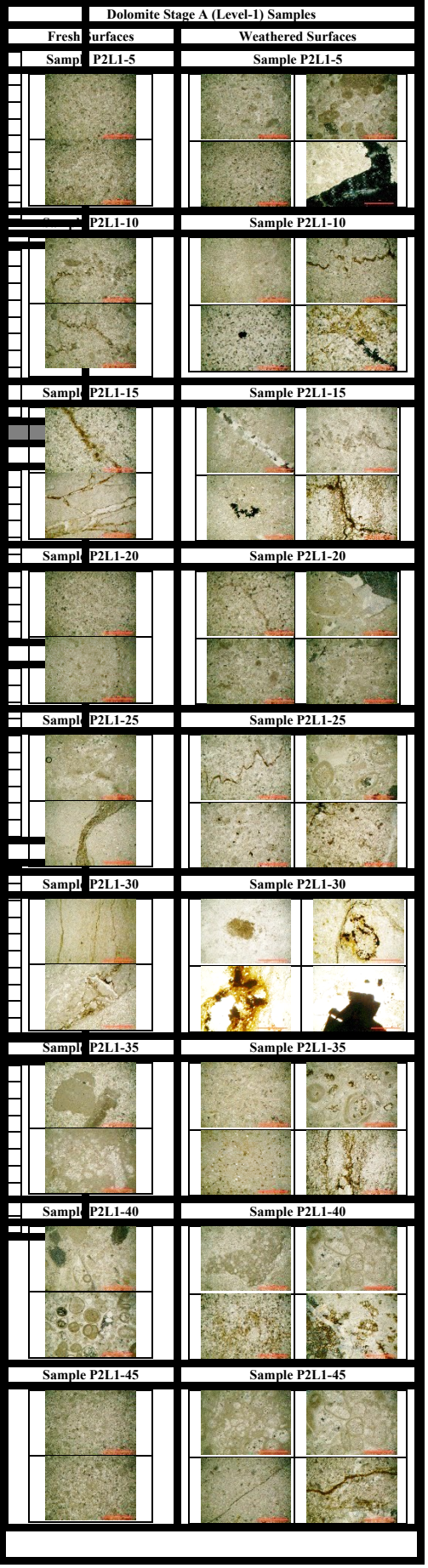

4. Results and Discussion

Based on the evaluated image processing results and the corresponding UCS values, R vs UCS, G vs UCS, B vs UCS, H vs UCS, S vs UCS, and V vs UCS graphical representations are provided for the fresh surfaces (f-1 and f-2) and weathered surfaces (w-1, w-2, w-3, w-4) obtained from thin section images from 4 different levels of Dolomite Quarry (i.e. P2L1-L4). (See Figure 13-Figure 19 for Dolomite Quarry, Profile 2, Level 1, fresh surfaces f-1 and f-2 along with the weathered surfaces (w-1, w-2, w-3, w-4), and also additionally average values of RGB &HSV-UCS). (See Figure 20-Figure 26 for Dolomite Quarry, Profile 2, Level 2). (See Figure 27-Figure 32 for Dolomite Quarry, Profile 2, Level 3). (See Figure 33-Figure 40 for Dolomite Quarry, Profile 2, Level 4).

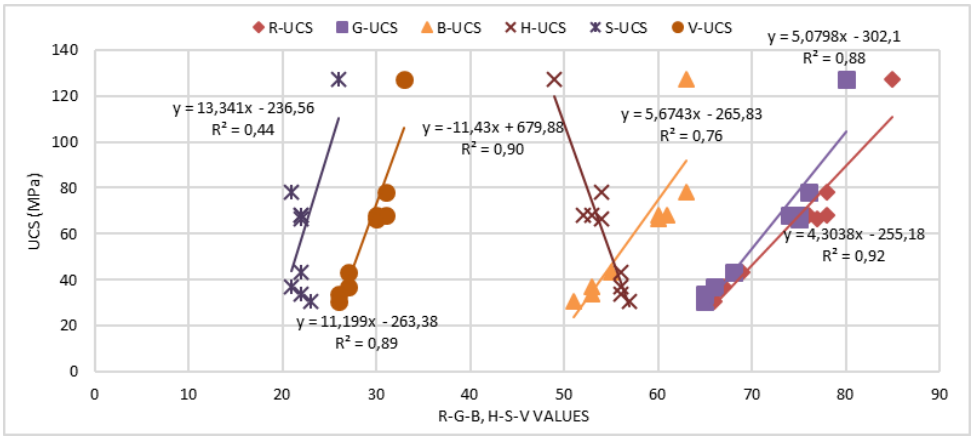

Fig. 13. P2L1 f-1 figure RGB-HSV&UCS

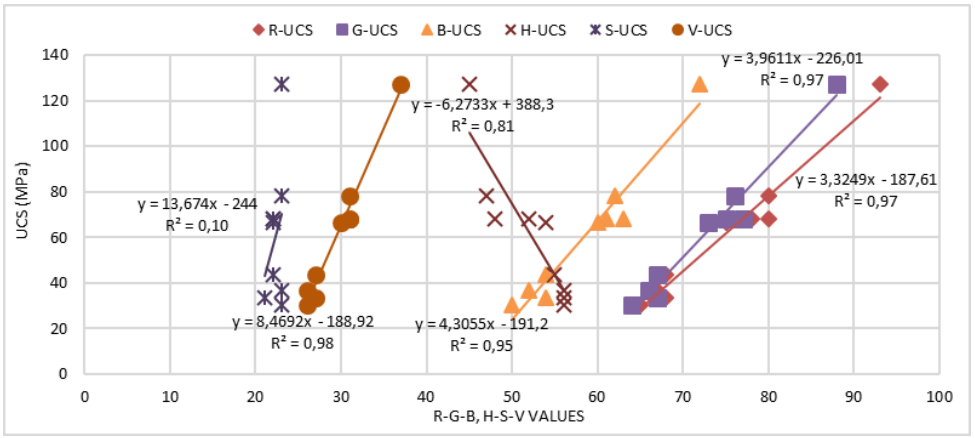

Fig. 14. P2L1 f-2 figure RGB-HSV&UCS

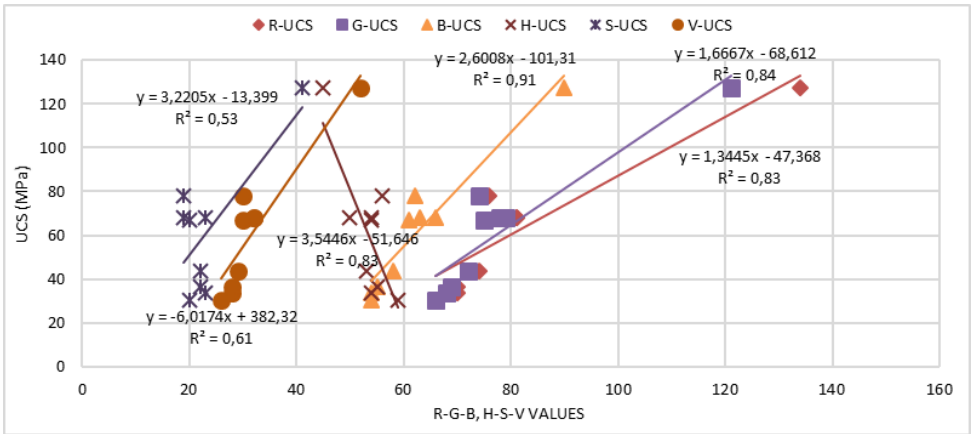

Fig. 15. P2L1 w-1 figure RGB-HSV&UCS

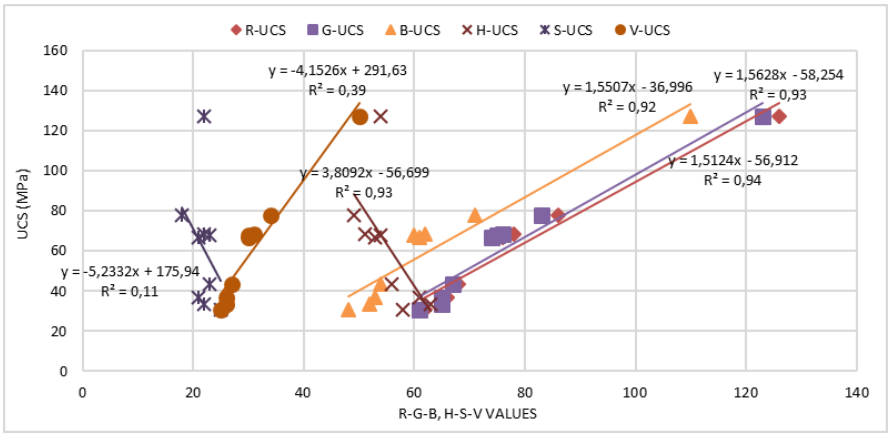

Fig. 16. P2L1 w-2 figure RGB-HSV&UCS

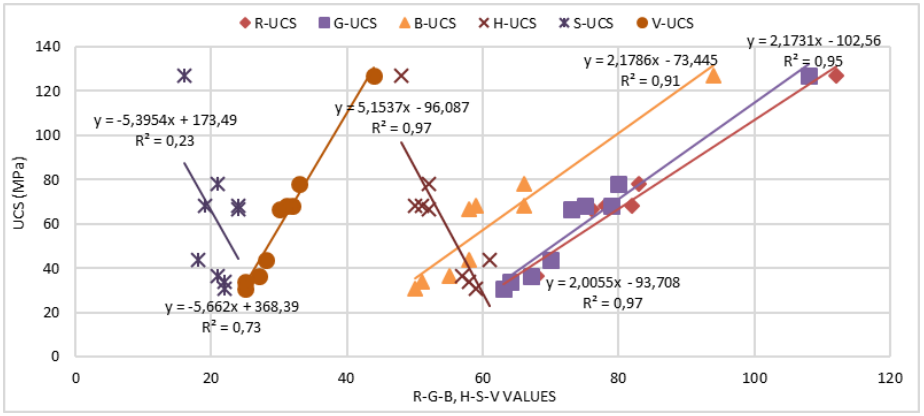

Fig. 17. P2L1 w-3 figure RGB-HSV&UCS

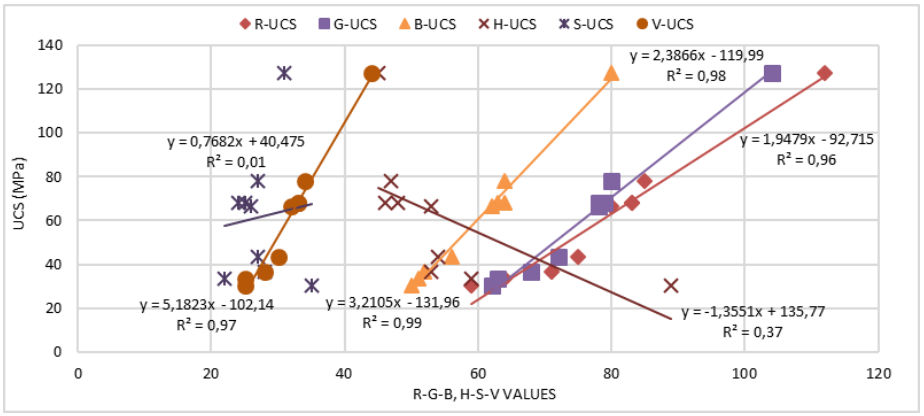

Fig. 18. P2L1 w-4 figure RGB-HSV&UCS

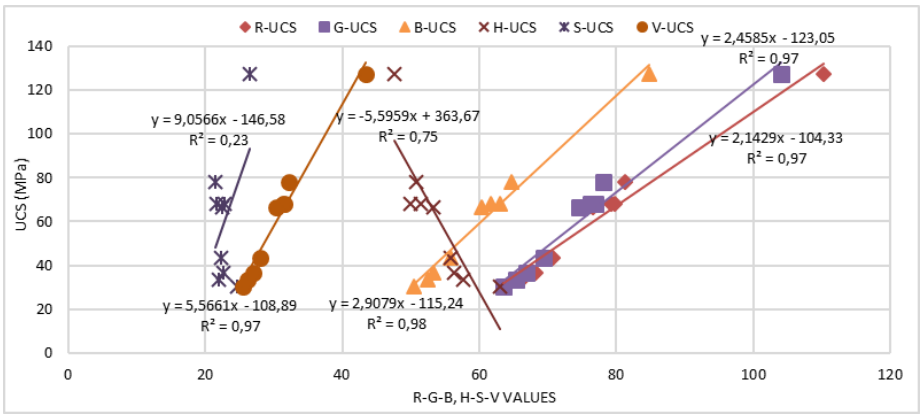

Fig. 19. P2L1 average figure RGB-HSV&UCS

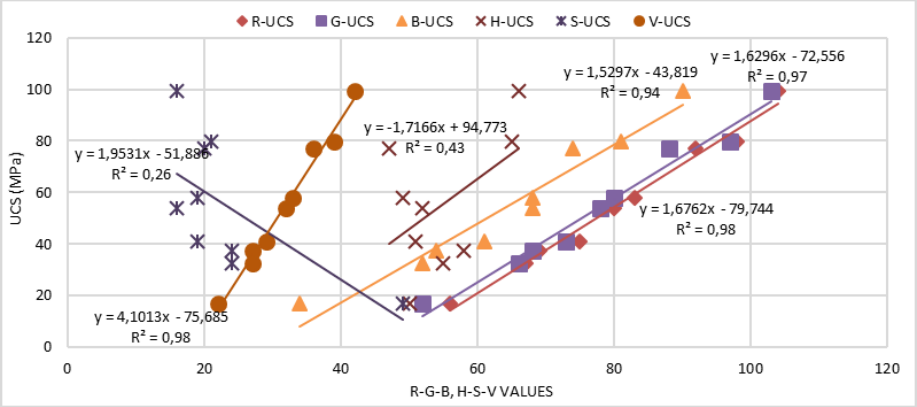

Fig. 20. P2L2 f-1 figure RGB-HSV&UCS

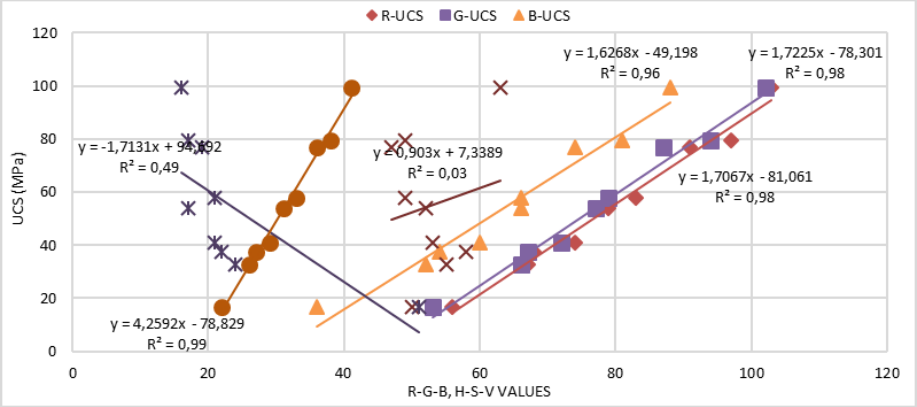

Fig. 21. P2L2 f-2 figure RGB-HSV&UCS

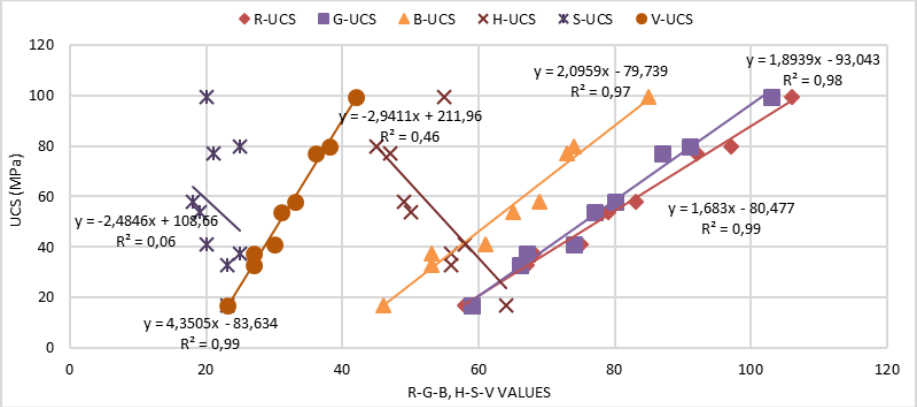

Fig. 22. P2L2 w-1 figure RGB-HSV&UCS

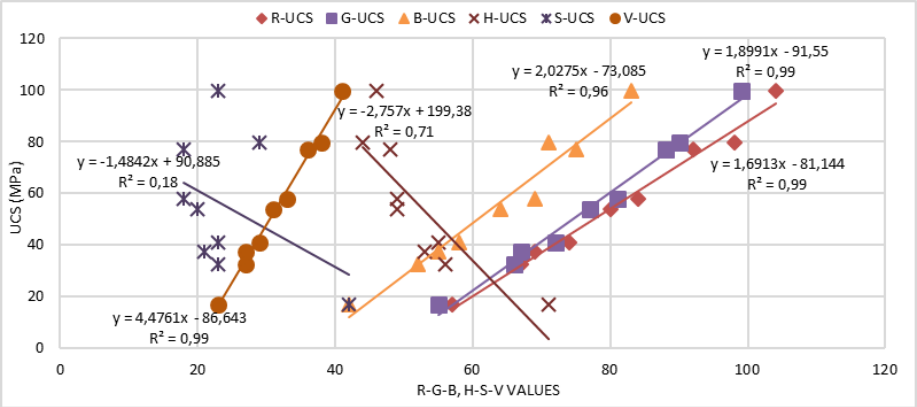

Fig. 23. P2L2 w-2 figure RGB-HSV&UCS

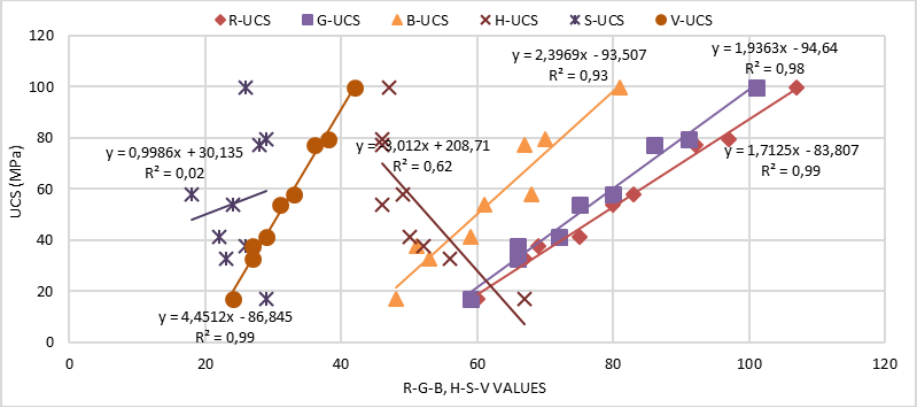

Fig. 24. P2L2 w-3 figure RGB-HSV&UCS

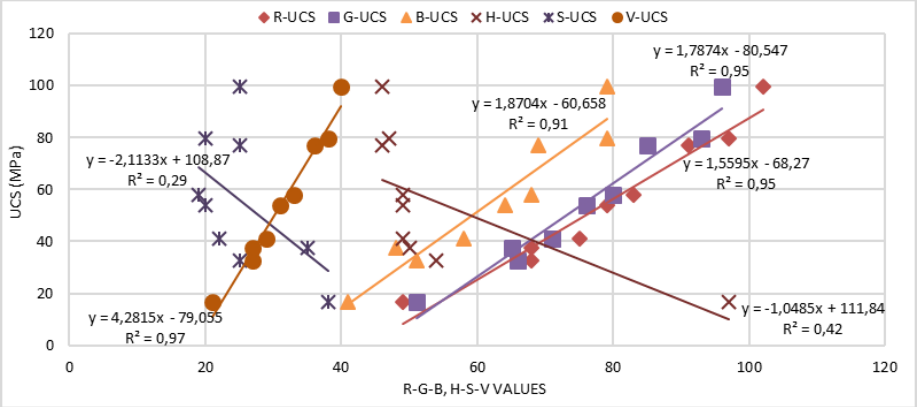

Fig. 25. P2L2 w-4 figure RGB-HSV&UCS

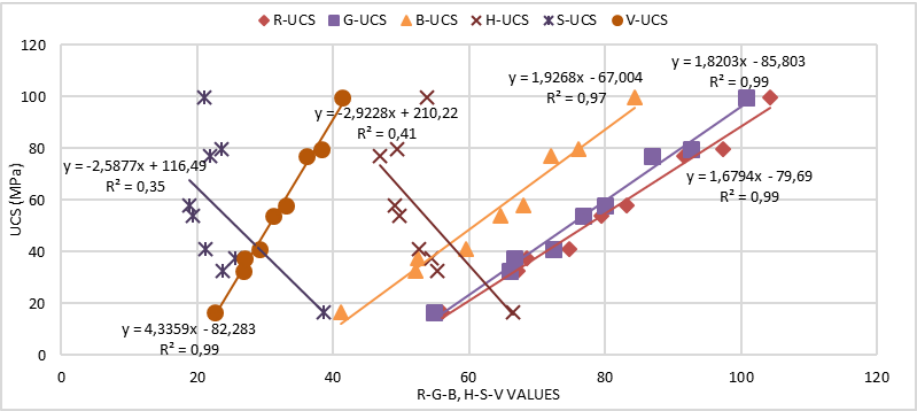

Fig. 26. P2L2 average figure RGB-HSV&UCS

Based on all of the abovementioned evaluated results obtained (See figures between Figure 13 and Figure 26), a summary of the datasheet including the correlation coefficients are provided in Table 2 in the case of the data obtained for Dolomite Stage A, P2L1.

Tab. 2. Summary of the datasheet including the correlation coefficients obtained from the interrelationships between image processing results and UCS (Dolomite Stage A, P2L1).

	Correlation Coefficient (R^2)					
	R	**G**	**B**	**H**	**S**	**V**
Fresh Surface-1 (f-1)	0,9214	0,8771	0,761	0,9031	0,4352	0,8859
Fresh Surface-2 (f-2)	0,9684	0,9681	0,9518	0,8066	0,1016	0,9764
Weathered Surface-1 (w-1)	0,8287	0,8437	0,9117	0,6099	0,5291	0,8275
Weathered Surface-1 (w-2)	0,9449	0,9316	0,9186	0,3893	0,1075	0,9342
Weathered Surface-1 (w-3)	0,9736	0,9533	0,9096	0,7296	0,2276	0,9749
Weathered Surface-1 (w-4)	0,9601	0,9764	0,9878	0,3679	0,0096	0,9712
Average Values ((f-1), (f-2), (w-1), (w-3), (w-4))	0,9732	0,9700	0,9806	0,7489	0,2326	0,9738

Schmidt Hammer Rebound (SHR) values and Uniaxial Compressive Strength (UCS) values are presented in Table 3 (left column) for Dolomite Stage B (P2L2), with the corresponding thin section images provided on the right. In addition, the RGB and HSV values derived from these images are tabulated in the middle column of Table 3 and Table 4.

Tab. 3. SHR values & UCS values tabulated in the study of Bilen (2021), thin section images of Dolomite Stage B, P2L2.

SHR and USC Results (Bilen 2021)

Schmidt Point	Average SHR value	UCS Value
P2L2-1	25	
P2L2-2	28.2	
P2L2-3	29.6	
P2L2-4	27.6	
P2L2-5	35.6	79,67
P2L2-6	24.6	
P2L2-7	36.2	
P2L2-8	25.8	
P2L2-9	25.4	
P2L2-10	31.8	53,75
P2L2-11	21.8	
P2L2-12	21	
P2L2-13	28.4	
P2L2-14	31.8	
P2L2-15	39.2	99,52
P2L2-16	28.6	
P2L2-17	27.2	
P2L2-18	33.6	
P2L2-19	26.8	
P2L2-20	19.4	16,73
P2L2-21	33	
P2L2-22	24.8	
P2L2-23	24.2	
P2L2-24	24.8	
P2L2-25	30	37,53
P2L2-26	34.2	
P2L2-27	34.6	
P2L2-28	38.2	
P2L2-29	34	
P2L2-30	31.8	57,94
P2L2-31	29.2	
P2L2-32	30.2	
P2L2-33	27.6	
P2L2-34	36.2	
P2L2-35	34.2	77,02
P2L2-36	43.8	
P2L2-37	29.4	
P2L2-38	37	
P2L2-39	33.6	
P2L2-40	34	41,05
P2L2-41	31.8	
P2L2-42	39.2	
P2L2-43	22	
P2L2-44	35.2	
P2L2-45	30.8	32,69

Sample Representation Fresh Surfaces		Sample Representation Weathering Surfaces	
f-1		w-1	w-2
f-2		w-3	w-4

Image Analysis of Thin Sections

Fresh Surfaces (f-1)

P2	R	G	B	H	S	V
L2-5	98	97	81	65	21	3
L2-10	80	78	68	52	16	3
L2-15	104	103	90	66	16	4
L2-20	56	52	34	50	49	2
L2-25	69	68	54	58	24	2
L2-30	83	80	68	49	19	3
L2-35	92	88	74	47	20	3
L2-40	75	73	61	51	19	2
L2-45	67	66	52	55	24	2

Fresh Surfaces (f-2)

P2	R	G	B	H	S	V
L2-5	97	94	81	49	17	3
L2-10	79	77	66	52	17	3
L2-15	103	102	88	63	16	4
L2-20	56	53	36	50	51	2
L2-25	68	67	54	58	22	2
L2-30	83	79	66	49	21	3
L2-35	91	87	74	47	19	3
L2-40	74	72	60	53	21	2
L2-45	67	66	52	55	24	2

Weathered Surfaces (w-1)

P2	R	G	B	H	S	V
L2-5	97	91	74	45	25	3
L2-10	79	77	65	50	19	3
L2-15	106	103	85	55	20	4
L2-20	58	59	46	64	23	2
L2-25	68	67	53	56	25	2
L2-30	83	80	69	49	18	3
L2-35	92	87	73	47	21	3
L2-40	75	74	61	58	20	3
L2-45	67	66	53	56	23	2

Weathered Surfaces (w-2)

P2	R	G	B	H	S	V
L2-5	98	90	71	44	29	3
L2-10	80	77	64	49	20	3
L2-15	104	99	83	46	23	4
L2-20	57	55	42	71	42	2
L2-25	69	67	55	53	21	2
L2-30	84	81	69	49	18	3
L2-35	92	88	75	48	18	3
L2-40	74	72	58	55	23	2
L2-45	67	66	52	56	23	2

Weathered Surfaces (w-3)

P2	R	G	B	H	S	V
L2-5	97	91	70	46	29	3
L2-10	80	75	61	46	24	3
L2-15	107	101	81	47	26	4
L2-20	60	59	48	67	29	2
L2-25	69	66	51	52	26	2
L2-30	83	80	68	49	18	3
L2-35	92	86	67	46	28	3
L2-40	75	72	59	50	22	2
L2-45	67	66	53	56	23	2

Weathered Surfaces (w-4)

P2	R	G	B	H	S	V
L2-5	97	93	79	47	20	3
L2-10	79	76	64	49	20	3
L2-15	102	96	79	46	25	4
L2-20	49	51	41	97	38	2
L2-25	68	65	48	50	35	2
L2-30	83	80	68	49	19	3
L2-35	91	85	69	46	25	3
L2-40	75	71	58	49	22	2
L2-45	68	66	51	54	25	2

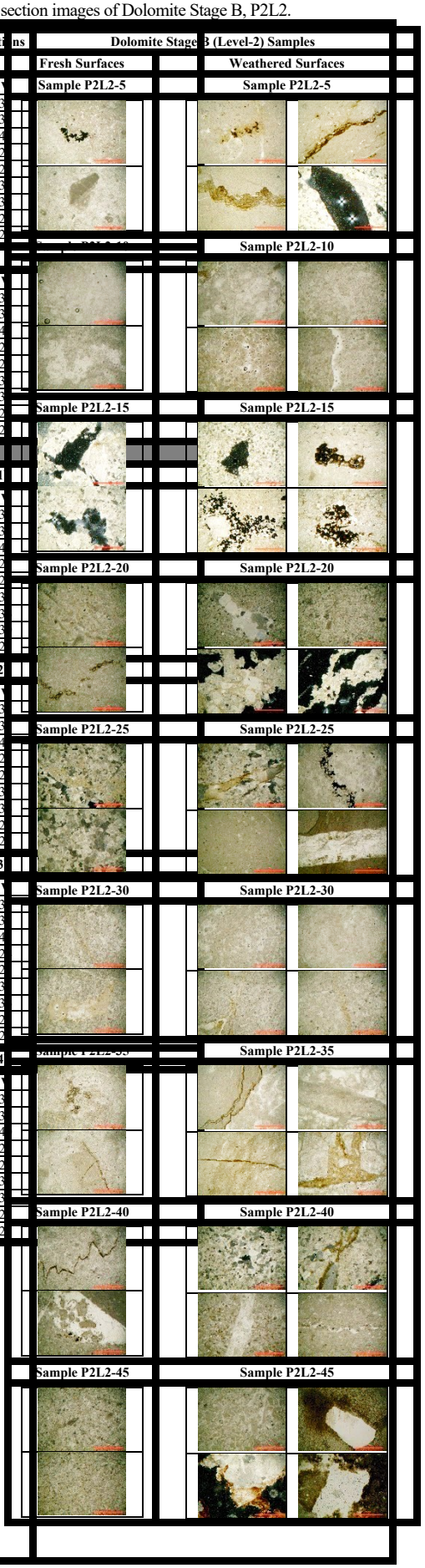

Tab. 4. Summary of the datasheet including the correlation coefficients obtained from the interrelationships between image processing results and UCS (Dolomite Stage B, P2L2).

	Correlation Coefficient (R^2)					
	R	**G**	**B**	**H**	**S**	**V**
Fresh Surface-1 (f-1)	0,9837	0,9737	0,9473	0,2610	0,4360	0,9850
Fresh Surface-2 (f-2)	0,9838	0,9831	0,9622	0,0304	0,4924	0,9883
Weathered Surface-1 (w-1)	0,9896	0,9837	0,9676	0,4553	0,0581	0,9856
Weathered Surface-1 (w-2)	0,9860	0,9878	0,9600	0,7124	0,1782	0,9895
Weathered Surface-1 (w-3)	0,9912	0,9840	0,9258	0,6182	0,0191	0,9889
Weathered Surface-1 (w-4)	0,9516	0,9542	0,9086	0,4195	0,2916	0,9715
Average Values ((f-1), (f-2), (w-1), (w-3), (w-4))	0,9862	0,9859	0,9692	0,4147	0,3467	0,9892

The results of the present study unequivocally demonstrate a consistent and robust relationship between RGB–HSV color parameters derived from thin-section images and the uniaxial compressive strength (UCS) of dolomitic rocks sampled from the Dolomite Quarry. Across the two stratigraphic levels investigated (P2L1–L2), statistical analyses revealed that correlation coefficients (R^2) derived from both fresh and weathered surfaces were remarkably high, particularly for the R, G, B, and V parameters. This finding is of significant importance, as it indicates that colorimetric indicators extracted from microscopic petrographic images are not merely qualitative descriptors of mineralogical change but are also quantitatively robust proxies for rock strength.

The comprehensive analysis of Tables 1, 2, 3, and 4, supported by detailed visualizations in Figures 13–26, highlights the systematic strength of R, G, B, and V parameters in capturing UCS variability. In Stage A (P2L1, Table 2), the average correlation coefficient between R and UCS was 0.9732, while G and V yielded comparably strong relationships (0.9700 and 0.9738, respectively). These values, which approach unity, emphasize that color intensities measured in digital space can explain nearly the entire variability in compressive strength for fresh dolomite surfaces. In Stage B (P2L2, Table 4), both fresh and weathered samples showed R^2 values consistently above 0.98 for R, G, and V parameters, demonstrating the reproducibility and robustness of the method across varying weathering intensities.

By contrast, the H (hue) and S (saturation) parameters consistently produced weaker correlations ($R^2 < 0.40$ in most cases). This observation aligns with the understanding that hue and saturation are more susceptible to lighting variations and surface effects rather than intrinsic mineralogical content. These findings resonate with earlier observations by Yusoff et al. (2021) and Gökay (2018), who noted that brightness and intensity changes are more diagnostic of mechanical degradation than tonal variations.

Figures 13–26 provide critical visual confirmation of how weathering modifies both color signatures and their correlation with UCS. Fresh surfaces (f-1, f-2) invariably exhibited stronger and more stable relationships, reflecting the homogeneity of unaltered dolomite microstructures. Weathered surfaces (w-1 to w-4) introduced some fluctuation due to mineralogical heterogeneity, dissolution voids, and clay/oxide accumulations. However, the diagnostic parameters—particularly R, B, and V—retained correlations above 0.90 in many weathered cases.

The transition from gray and bluish-gray hues in fresh dolomite to yellowish-brown tones in weathered specimens, as also observed in field descriptions (Figures 8–9), is directly associated with reductions in UCS. This colorimetric transformation is caused by oxidation, clay enrichment, and porosity development, which weaken the rock fabric. Thus, RGB–HSV analysis captures the mineralogical and textural transformations that directly control mechanical strength, confirming the visual engineering indicators proposed by Fookes et al. (1971) and Ündül and Tuğrul (2012).

Validation of the image-based approach against independent strength tests further enhances its credibility. Table 1 and 3 provide UCS and Schmidt Hammer Rebound (SHR) results that parallel the RGB–HSV outcomes. For instance, SHR values in Stage A (Table 1) show systematic decreases alongside UCS reductions, directly matching the attenuation of R and V color intensities. Similarly, in Stage B (Table 3), the correspondence between UCS–SHR values and RGB–HSV-derived predictions confirms that the method does not simply capture superficial discoloration, but accurately reflects underlying mechanical degradation processes. This integrative validation builds upon previous findings by Singh and Gahrooee (1989) and Hack and Price (1997), who also emphasized the potential of indirect methods for weathering and strength assessment.

The engineering implications of these findings are profound, particularly for tunneling projects employing Tunnel Boring Machines (TBMs). As established by Thuro and Spaun (1996), Khetwal et al. (2020), and Li et al. (2021), TBM performance—penetration rate, cutter wear, and advance speed—is strongly governed by UCS, weathering degree, and rock heterogeneity. However, traditional UCS testing is time-consuming and impractical for real-time applications. The present study demonstrates that RGB–HSV color analysis, when integrated into TBM monitoring systems, can provide a rapid, non-destructive, and cost-effective proxy for UCS.

As proposed by Li et al. (2023) and Zhu et al. (2025), cameras mounted on TBM cutterheads or conveyor systems could continuously capture face and muck images. These images, processed in real time, would yield RGB–HSV data that can be translated into UCS predictions, thereby enabling adaptive adjustments in cutterhead tool selection, operational parameters, and maintenance schedules. Such integration would minimize tool wear, reduce downtime, and enhance overall excavation safety and efficiency. Moreover, in heterogeneous carbonate environments like the Gebze region, where weathering can vary sharply across short distances, this method offers unparalleled advantages in adaptive excavation planning.

The strong correlations observed in this study resonate with decades of research on weathering–strength interactions in carbonate rocks. Fookes et al. (1971) emphasized that weathering significantly reduces UCS in carbonates. Singh and Gahrooee (1989) and Hack and Price (1997) demonstrated that indirect methods could approximate weathering grades. However, these methods often suffer from limitations in speed and field applicability. The RGB–HSV-based methodology presented here directly addresses these shortcomings, providing a reproducible, quantitative, and field-deployable solution.

Furthermore, the results align with advances in digital image processing and machine learning applications in rock mechanics. dos Anjos et al. (2021), Zhao et al. (2021), and Tembely et al. (2021) have shown that high-resolution image data can successfully predict mechanical behavior at macroscopic scales. The present study confirms that RGB–HSV metrics, even without complex machine learning models, can serve as robust strength predictors, opening avenues for integration with intelligent excavation tool-support systems.

Taken together, the correlation coefficients documented in Tables 2 and 4, along with graphical evidence from Figures 13–26, conclusively demonstrate that RGB and V parameters serve as reliable and robust predictors of UCS across varying degrees of weathering.

Independent validation through SHR and UCS testing (Tables 1 and 3) further strengthens this conclusion. This integrative framework confirms that RGB–HSV analysis is not only a scientifically valid but also an engineering practical approach.

The broader contribution of this study lies in bridging laboratory-based petrographic analysis with field-applicable as exvataion tool. By transforming thin-section colorimetric data into predictive strength metrics, the method enables real-time estimation of rock mass conditions during tunneling. Its implications extend beyond academic research, providing tangible benefits in equipment optimization, excavation efficiency, and safety management. Ultimately, this approach represents a paradigm shift in tunneling operations, where color-based digital imaging can be systematically harnessed for predictive geomechanical modeling in carbonate rock environments.

5. Conclusion

This study has demonstrated the feasibility and effectiveness of applying RGB image-based classification to evaluate weathering-induced changes in dolomites of the Gebze region, with a specific focus on their implications for excavation tool optimization in tunnel engineering. By integrating petrographic thin-section analyses, Schmidt Hammer Rebound (SHR) values, and Uniaxial Compressive Strength (UCS) measurements with systematic RGB–HSV image processing, the research establishes clear and statistically significant correlations between microstructural color variations and rock mechanical behavior across fresh and weathered states.

The results confirm that RGB color metrics are highly sensitive to mineralogical transformations, dissolution features, and secondary infillings that develop during progressive weathering. These variations directly translate into measurable differences in strength and drillability, underscoring the capacity of image-based approaches to capture geotechnically relevant information that traditional field observations often overlook. The high correlation coefficients obtained, particularly for fresh and moderately weathered samples, indicate that RGB parameters can serve as reliable proxies for mechanical strength, reducing the need for labor-intensive and costly laboratory testing.

From an engineering perspective, the integration of RGB-based classification into tunnel boring machine (TBM) systems offers significant advantages. Real-time capture and processing of color data at the excavation face enables the anticipation of lithological transitions and weathering zones, allowing for proactive tool selection, reduced cutter wear, and improved excavation stability. This adaptive capability addresses one of the key challenges in carbonate tunneling projects, where localized heterogeneity in weathering can otherwise cause abrupt performance losses and safety risks.

The broader contribution of this work lies in presenting a low-cost, rapid, and scalable methodological framework that bridges petrographic detail with engineering decision-making. Beyond its immediate application in tunnel engineering, the approach may be extended to other fields requiring rapid assessment of carbonate rock integrity, including slope stability, foundation design, and quarry resource management. Future studies should explore coupling RGB-based classification with machine learning algorithms and hyperspectral imaging to further refine predictive models and enhance robustness under variable field conditions.

In conclusion, this research provides convincing evidence that RGB image-based weathering classification is not only scientifically valid but also practically transformative. By aligning petrographic insights with engineering performance metrics, it lays the groundwork for next-generation adaptive excavation systems capable of responding intelligently to complex subsurface conditions, thereby improving efficiency, safety, and sustainability in underground construction projects.

Acknowledgements

The author gratefully acknowledge the owners and operators of the limestone-dolomite quarries for their generous support in providing the rock samples essential for this research. Sincere appreciation is also extended to the Head of the Department of Mining Engineering, Faculty of Engineering, Zonguldak Bülent Ecevit University, for granting access to the image processing facilities and the Rock Mechanics Laboratory, which greatly contributed to the successful completion of this study.

References

1. Abad SVANK, Mohamad ET, Komoo I, Kalatehjari R (2015) Assessment of weathering effects on rock mass structure. Jurnal Teknologi, 72(1). https://doi.org/10.11113/jt.v72.2875.
2. Akyıldırım H, Karakaş A (2021) Kocaeli-Gebze Tavşanli Bölgesi Kireçtaşlarinin Beton Agregası Olarak Kullanilabilirliğinin Araştirilmasi. Konya Journal of Engineering Sciences 9(4):1088-1108. https://doi.org/10.36306/konjes.925801
3. Alavi Nezhad Khalil Abad SV, Mohamad ET, Komoo I (2014) Dominant weathering profiles of granite in southern Peninsular Malaysia. Eng Geol 2014;183:208–15. doi: https://doi.org/10.1016/j.enggeo.2014.10.019.
4. Alavi Nezhad Khalil Abad SV, Mohamad ET, Komoo I, Kalatehjari R (2015) A typical weathering profile of granitic rock in Johor, Malaysia based on joint characterization. Arabian Journal of Geosciences, 8(4), 2191–2201. https://doi.org/10.1007/s12517-014-1345-7
5. Alavi Nezhad Khalil Abad SV, Tugrul A, Gokceoglu C, Jahed Armaghani D (2016). Characteristics of weathering zones of granitic rocks in Malaysia for geotechnical engineering design. Engineering Geology, 200, 94–103. https://doi.org/10.1016/j.enggeo.2015.12.006
6. Altınlı E (1968) İzmit-Hereke-Kurucadağ alanının jeoloji incelemesi. MTA Derg (71):1-26 (in Turkish).
7. Amankwah A, Aldrich C (2011) Automatic estimation of rock particulate size on conveyer belt using image analysis. In International Conference on Graphic and Image Processing (ICGIP 2011) (Vol. 8285, pp. 347-354). SPIE.
8. Arman H, Hussein S, Abouhaligah HEY, Osman M, Baloch MA, Hag DBA, Algaishi HAA (2019) Predicting Weathering Characteristics of Carbonate Rocks Under Different Geo-Environmental Conditions. In IOP Conference Series: Earth and Environmental Science (Vol. 362, No. 1, p. 012016). IOP Publishing. https://doi:10.1088/1755-1315/362/1/012016
9. ASTM (2001) Standard test method for determination of rock hardness by rebound hammer method ASTM Stand., 04.09 (2001) (D 5873-00).

10. Azarafza M, Koçkar MK, Faramarzi L (2021) Spacing and block volume estimation in discontinuous rock masses using image processing technique: A case study. Environmental Earth Sciences, 80. https://doi.org/10.1007/s12665-021-09768-3
11. Bagheri GH, Bonadonna C, Manzella I, Vonlanthen P (2015) On the characterization of size and shape of irregular particles. Powder Technology, 270, 141-153. https://doi.org/10.1016/j.powtec.2014.10.015
12. Barla G, Forlati F, Zaninetti A (1990) Laboratory tests on rocks: issues and examples. MIR 90. Torino 4-1:4–47.
13. Bhatawdekar RM, Edy MT, Danial JA (2019) Building information model for drilling and blasting for tropically weathered rock. Journal of Mines, Metals and Fuels. 67 (11):494-500.
14. Bilen C (2020) Classification and Characterization of Weathered Limestones, PhD Thesis, Istanbul Universirty-Cerrahpasa, 159 p.
15. Bilen C (2021) Schmidt Hammer Rebound (SHR) values as a guide for the initial estimates of limestone uniaxial compressive strength (UCS) and Hardgrove grindability index (HGI). Arabian Journal of Geosciences, 14, 1-15. https://doi.org/10.1007/s12517-021-08421-4
16. Bilen C, Sakız (2023) The effect of weathering on drillability of dolomites. Open Geosciences, vol. 15, no. 1, pp. 20220568. https://doi.org/10.1515/geo-2022-0568
17. Bilen C, Tuğrul A, Ündül Ö (2025) Engineering geological evaluation of weathered limestones and dolomites quarries in Gebze (Türkiye).Bull Eng Geol Environ 84, 227. https://doi.org/10.1007/s10064-025-04245-8
18. Bieniawski ZT (1984) Rock Mechanics design in mining and tunneling. Balkema, Boston.
19. Blyth FGH, de Freitas MH (1984) A geology for engineers. Elsevier 7th Edition, 336p. London.
20. Capik M, Yilmaz AO, Yasar S (2017) Relationships between the drilling rate index and physicomechanical rock properties. Bull Eng Geol Environ. 76:253-61. https://doi.org/10.1007/s10064-016-0991-2
21. Casali G, Vallebuona C, Pérez G, González R, Vargas L (2000) Lithological composition and ore grindability sensors based on image analysis, in: Proceedings of the XXI IMPC, Rome, pp. A1(9–16).10. Azarafza M, Koçkar MK, Faramarzi L (2021) Spacing and block volume estimation in discontinuous rock masses using image processing technique: A case study. Environmental Earth Sciences, 80. https://doi.org/10.1007/s12665-021-09768-3
22. Ceryan N, Ozkat EC, Korkmaz Can N, Ceryan S (2021) Machine learning models to estimate the elastic modulus of weathered magmatic rocks. Environmental Earth Sciences, 80(12), 448. https://doi.org/10.1007/s12665-021-09738-9
23. Chai SYW, Damu DNA, How BS, Chin MY, Adini M, Anong JB, Chin MY, Adini MJBA, Kassim AM, Peter C, Ngu LH (2024) Optimization of accelerated weathering of limestone for CO2 capture in cement industry. In AIP Conference Proceedings (Vol. 3041, No. 1). AIP Publishing. https://doi.org/10.1063/5.0194621
24. Chang C, Beckford HO, Ji H (2022) Indication of Sr Isotopes on Weathering Process of Carbonate Rocks in Karst Area of Southwest China. Sustainability 14(8), 4822. https://doi.org/10.3390/su14084822
25. Chen Z, Zhang Y, Li J, Li X, Jing L (2021) Diagnosing tunnel collapse sections based on TBM tunneling big data and deep learning: A case study on the Yinsong Project, China. Tunnelling and Underground Space Technology, 108, 103700. https://doi.org/10.1016/j.tust.2020.103700
26. Chiu CF, Ng CWW (2014) Relationships between chemical weathering indices and physical and mechanical properties of decomposed granite. Eng Geol, 179:76–89. doi: https://doi.org/10.1016/j.enggeo.2014.06.021
27. Cleland TM (1921) Practical description of the Munsell color system, with suggestions for its use.
28. Connolly C, Fleiss T (1997) A study of efficiency and accuracy in the transformation from RGB to CIELAB color space. IEEE Trans Image Process. 6(7):1046–8. doi: https://doi.org/10.1109/83.597279.
29. Da Fonseca BS, Pinto AF, Rodrigues A, Picarra S, Fonseca D, Montemor MF (2021) On the estimation of marbles weathering by thermal action using drilling resistance. J Build Eng.;42:102494. https://doi.org/10.1016/j.jobe.2021.102494
30. Dobereiner L (1984) Engineering geology of weak sandstones [PhD thesis]. University of London, p 471.
31. Dong X, Cohen MJ, Martin JB, McLaughlin DL, Murray AB, Ward ND, Flint MK, Heffernan JB (2018) Ecohydrologic processes and soil thickness feedbacks control limestone-weathering rates in a karst landscape. Chemical Geology. https://doi.org/10.1016/j.chemgeo.2018.05.021
32. dos Anjos CE, Avila MR, Vasconcelos AG, Pereira Neta AM, Medeiros LC, Evsukoff AG, Surmas R, Landau L (2021) Deep learning for lithological classification of carbonate rock micro-CT images. Computational Geosciences, 25, 971-983. https://doi.org/10.1007/s10596-021-10033-6
33. Dunham RJ (1962) Classification of carbonate rocks according to depositional texture.
34. Dursun G (2004) The evaluation of limestones in Anatolian part of Istanbul from the point of aggregate quality. Master Thesis, Istanbul University (in Turkish).

35. Embry AF, Klovan JE (1971) A late Devonian reef tract on Northeastern Banks Island, NWT. Canadian Petroleum Geology Bulletin, 19, 730–781. https://doi.org/10.35767/gscpgbull.19.4.730

36. Erguvanlı K (1949) Hereke pudingleri ile Gebze taşları-inşaat bakımından etüdü ve civarlarının jeolojisi. PhD thesis, ITU, (in Turkish).

37. Erkol D, Aydındağ A (2012) Gebze (Kocaeli) Agrega-Kırmataş Maden Jeolojisi, MTA Doğa Kaynakları ve Ekonomi Bülteni 16:241-243 (in Turkish).

38. Ersöz T, Topal T (2018) Weathering and Excavation Effects on the Stability of Various Cut Slopes in Flysch-Like Deposits. Geotech Geol Eng 36, 3707–3729. https://doi.org/10.1007/s10706-018-0566-z

39. Fan K (2025) Advancements in digital drilling technology for deep engineering: a review. Frontiers in Earth Science, 13, 1604584.

40. Farrokh E, Rostami J (2008) Correlation of tunnel convergence with TBM operational parameters and chip size in the Ghomroud tunnel, Iran. Tunnelling and Underground Space Technology, 23(6), 700-710.

41. Felekoglu B (2007) Utilisation of high volumes of limestone quarry wastes in concrete industry (self-compacting concrete case). Resources, Conservation and Recycling, 51(4), 770-791. https://doi.org/10.1016/j.resconrec.2006.12.004

42. Fookes PG, Dearman WR, Franklin JA (1971) Some engineering aspects of rock weathering with field examples from Dartmoor and elsewhere. Quarterly Journal of Engineering Geology and Hydrogeology 4(3):139-185. https://doi.org/10.1144/GSL.QJEG.1971.004.03.01

43. Fu H, Jian X, Pan H (2023) Bias in sediment chemical weathering intensity evaluation: a numerical simulation study. Earth-Science Reviews 104574. https://doi.org/10.1016/j.earscirev.2023.104574

44. Gedik İ, Duru M, Pehlivan Ş, Timur, E (2005) 1/50.000 ölçekli Türkiye Jeoloji haritaları, İstanbul-F22c Paftasi. MTA Raporu No:11, Ankara (in Turkish).

45. Gong Q, Zhou X, Liu Y, Han B, Yin L (2021) Development of a real-time muck analysis system for assistant intelligence TBM tunnelling. Tunnelling and Underground Space Technology, 107, 103655.

46. Gonzalez de Vallejo LI, Ferrer M, Ortuño L, Oteo C (2002) Ingeneria geologica. Pearson Education, Madrid, p 744.

47. Gökay MK (2018) Analyses of rock surface colour changes due to weathering. Scitech; 6(1):11–13.

48. Grossi D, Lama EA Del, García Talegón J, Iñigo AC, Iñigo AC, Vicente Tavera S (2015) Evaluation of colorimetric changes in the itaquera granite of the Ramos de Azevedo Monument, São Paulo, Brazil.

49. Hack R, Price D. (1997) Quantification of weathering. Engineering Geology and the Environment proceedings. Athens.

50. Henley KJ (1983) Ore-dressing mineralogy—a review of techniques, applications and recent developments, Special Publication - Geological Society of South Africa, 7, 175–200.

51. Heydari S, Hamidi JK, Monjezi M, Eftekhari A (2019) An investigation of the relationship between muck geometry, TBM performance, and operational parameters: A case study in Golab II water transfer tunnel. Tunnelling and Underground Space Technology, 88, 73-86.

52. Howarth DF, Adamson WR, Berndt JR. (1986) Correlation of model tunnel boring and drilling machine performances with rock proporties. Int J Rock Mech Min Sci., 23(2):57–85. https://doi.org/10.1016/0148-9062(86)90344-X

53. Huang MQ, Ninić J, Zhang Q (2021) BIM, machine learning and computer vision techniques in underground construction: Current status and future perspectives. Tunnelling and Underground Space Technology, 108, 103677.

54. Irfan TY, Dearman WR (1978) The engineering petrography of a weathered granite in Cornwall, England. Q J Eng Geol Hydrogeol (11):233-244. https://doi.org/10.1144/GSL.QJEG.1978.011.03.03

55. Ismail A, Rashid ASA, Sa'Ari R, Rasib AW (2020) Application of photogrammetric technique in determination of rock slope stability of quarry. In IOP Conference Series: Materials Science and Engineering (Vol. 932). https://doi.org/10.1088/1757-899X/932/1/012054

56. ISRM (2007) The complete ISRM suggested methods for rock characterization, testing and monitoring: 1974–2006. In: Ulusay R, Hudson JA (eds) Suggested methods prepared by the commission on testing methods, International Society for Rock Mechanics, Compilation Arranged by the ISRM Turkish National Group, Kozan Ofset, Ankara, Turkey

57. Jennings JE (1966) Building on dolomites in the Transvaal, civil engineering in South Africa. Trans South African Institute of Civil Engineering 8(2):41-62. https://hdl.handle.net/10520/AJA10212019_20409

58. Johnston IW (1993) Geomechanics and the emergence of soft rock technology. Australian Geomechanics, 3-13.

59. Jones MP, Horton R (1979) Recent development in the stereological assessment of composite (middlings) particles by linear measurements, in: M.J. Jones (Ed.), Proceedings of the XIth Commonwealth Mining and Metallurgical Congress, IMM, London, pp. 113–122.

60. Kahraman S (1999) Rotary and percussive drilling prediction using regression analysis. Int J Rock Mech Min Sci.; 36(7):981–9. https://doi.org/10.1016/S0148-9062(99)00050-9

61. Kanji MA (2014) Critical issues in soft rocks. J Rock Mech Geotech Eng 6(3):186–195.

62. Khan T, Shamim Khan M (2016) Geochemistry of the sandstones of Punagarh Basin: Implications for two source terranes and Arabian-Nubian connection of Aravalli Craton? Journal of the Geological Society of India, 88, 366–386. https://doi.org/10.1007/s12594-016-0499-1

63. Khetwal A, Rostami J, Nelson PP (2020) Investigating the impact of TBM downtimes on utilization factor based on sensitivity analysis. Tunnelling and Underground Space Technology, 106, 103586. https://doi.org/10.1016/j.tust.2020.103586

64. Komoo I (1995) Weathering as an important factor in assessing engineering properties of rock materials. Kuala Lumpur: Forum Soil Rock Prop. Geol. Soc. Malaysia. Univ. Malaya.

65. Küçükuysal C, Gül M, Aghayev T, Gülcan M (2022) Mineralogical and geochemical signatures of weathering on carbonate rocks and dynamic young land surfaces in Muğla Polje (SW Turkey). Turkish Journal of Earth Sciences 31(6):563-578. https://doi.org/10.55730/1300-0985.1820

66. Leu SS, Chang SL (2005) Digital image processing based approach for tunnel excavation faces. Automation in Construction, 14, 750–765. https://doi.org/10.1016/j.autcon.2005.02.004

67. Li S, Liu B, Xu X, Nie L, Liu Z, Song J, Chen L, Fan K (2017) An overview of ahead geological prospecting in tunneling. Tunnelling and Underground Space Technology, 63, 69-94. https://doi.org/10.1016/j.tust.2016.12.011

68. Li S, Ma C, Liu R, Chen M, Yan J, Wang Z, Duan S, Zhang H (2021) Super-absorbent swellable polymer as grouting material for treatment of karst water inrush. International Journal of Mining Science and Technology, 31(5), 753-763. https://doi.org/10.1016/j.ijmst.2021.06.004

69. Li X, Wu L, Wang Y, Li JH (2023) Rock fragmentation indexes reflecting rock mass quality based on real-time data of TBM tunnelling. Sci Rep 13, 10420. https://doi.org/10.1038/s41598-023-37306-7

70. Liang M, Mohamad ET, Komoo I, Chau-Khun M (2017) Performance evaluation of existing surface excavation assessment methods on weathered sedimentary rock. Bull Eng Geol Environ.;76:205–18. https://doi.org/10.1007/s10064-015-0771-4

71. Lin CL, Yen YK, Miller JD (1993) Evaluation of a PC image-based online coarse particle size analyzer, in: Proceedings of Emerging Computer Techniques for the Mineral Industry Symposium, AIME/SME, pp. 201–210.

72. Liu B, Wang Y, Zhao G, Yang B, Wang R, Huang D, Xiang B (2021) Intelligent decision method for main control parameters of tunnel boring machine based on multi-objective optimization of excavation efficiency and cost. Tunnelling and Underground Space Technology, 116, 104054.

73. Lopez BR, Bacilio M (2020) Weathering and soil formation in hot, dry environments mediated by plant–microbe interactions. Biol Fertil Soils 56, 447–459. https://doi.org/10.1007/s00374-020-01456-x

74. Luo JY, Xu ZM, Ren Z, Wang K, Gao HY, Yang K, Tang YJ, Tian L (2020) Quantitative assessment of weathering degree of the Touzhai rock-avalanche deposit in Southwest China. Geomorphology, 359. https://doi.org/10.1016/j.geomorph.2020.107162

75. Malamas M, Elias N, Petrakis EGM, Zervakis M, Petit L, Legat JD (2003) A survey on industrial vision systems, applications and tools, Image Vision Computing, 21(2) 171–188.

76. Mareš J, Weiss T, Wieler N, Shtober-Zisu N (2024) Climate controls on limestone cavernous weathering patterns in Israel. Geomorphology 462, 109334. https://doi.org/10.1016/j.geomorph.2024.109334

77. Marques EAG, Vargas EA, Leão MF (2020) Weathering of Rocks in Brazil. In: Kanji M, He M, Ribeiro e Sousa L (eds). Soft Rock Mechanics and Engineering 251-290 https://doi.org/10.1007/978-3-030-29477-9_10

78. Martínez-Martínez J, Berrezueta E, Aguilera H, Fusi N (2023) Aspect influence on the weathering micro-rates of limestones exposed under semiarid coastal Mediterranean climate. Construction and Building Materials 392, 131942. https://doi.org/10.1016/j.conbuildmat.2023.131942

79. Matsumoto S, Shimada H, Sasaoka T (2017) Interaction between physical and chemical weathering of argillaceous rocks and the effects on the occurrence of acid mine drainage (AMD). Geosci J (21):1-10. https://doi.org/10.1007/s12303-016-0064-3

80. McFeat-Smith I, Fowell RJ (1977) Correlation of rock properties and the cutting performance of tunneling machines. Proceedings of a Conference on Rock Engineering. London, UK: British Geotechnical Society.

81. Munsell AH, Nickerson D (1915) Munsell color system. Howland & Company, Incorporated: Wadsworth.

82. Murray RC (1960) Origin of porosity in carbonate rocks. J Sed Petrology (30): 59-84. https://doi.org/10.1306/74D709CA-2B21-11D7-8648000102C1865D

83. Nagano T, Nakashima S (1989) Study of colors and degrees of weathering of granitic rocks by visible diffuse reflectance spectroscopy. Geochemical Journal, 23(2), 75-83. https://doi.org/10.2343/geochemj.23.75

84. Ng CWW, Guan P, Shang YJ (2001) Weathering mechanisms and indices of the igneous rocks of Hong Kong. Q J Eng Geol Hydrogeol; 34(2):133–51. doi: https://doi.org/10.1144/qjegh.34.2.133

85. Oestreich J, Tolley W, Rice D (1995) The development of a color sensor system to measure mineral compositions, Minerals Engineering, 8(1/2) 31–39. https://doi.org/10.1016/0892-6875(94)00100-Q

86. Petersen KRP, Aldrich C, Vandeventer JSJ (1998) Analysis of ore particles based on textural pattern recognition, Minerals Engineering, 11(10) 959–977. https://doi.org/10.1016/S0892-6875(98)00083-1

87. Petruck W, Lastra R (1993) Evaluation of recovery of liberated and unliberated chalcopyrite by flotation columns in a copper cleaner circuit, International Journal of Mineral Processing, 40(1–2) 137–149. https://doi.org/10.1016/0301-7516(93)90046-D

88. Price JR, Velbel MA (2003) Chemical weathering indices applied to weathering profiles developed on heterogeneous felsic metamorphic parent rocks. Chemical Geology 202(3-4):397-416. https://doi.org/10.1016/j.chemgeo.2002.11.001

89. Puente ME, Rodríguez-Jaramillo MC, Li CY, Bashan Y (2006) Image analysis for quantification of bacterial rock weathering. J Microbiol Methods; 64 (2):275–86. doi: https://doi.org/10.1016/j.mimet.2005.05.007.

90. Rajabi AM, Hosseini A, Heidari A (2017) The new empirical formula to estimate the uniaxial compressive strength of limestone; north of saveh a case study. Journal of Engineering Geology, 11(3), 159.

91. Rocha M (1975) Some problems related to the rock mechanics of low strength natural materials. In Proceedings of the 5th Pan-American conference on soil mechanics and foundation engineering, Buenos Aires, pp 489–514.

92. Russo G (1994) Some considerations on the applicability of major geomechanical classifications to weak and complex rocks in tunnelling. GEAM 31:63–70.

93. Sarkar K, Singh AK, Niyogi A, Behera PK, Verma AK, Singh TN (2016) The assessment of slope stability along NH-22 in Rampur-Jhakri area, Himachal Pradesh. Journal of the Geological Society of India, 88, 387–393. https://doi.org/10.1007/s12594-016-0500-z

94. Saunders MK, Fookes PG (1970) A review of the relationship of rock weathering and climate and its significance to foundation engineering. Eng Geol.; 4(4):289–293, 299–25. https://doi.org/10.1016/0013-7952(70)90021-9

95. Service PT (2013) CIELAB System. Defining and Communicating Color : The CIELAB System. Sappi Fine Pap North Am 2013:1–8.

96. Shafarenko L, Petrou M, Kittler J (1997) Histogram-based segmentation in a perceptually uniform color space, IEEE Transactions on Image Processing, 7(9) 1354–1358. https://doi.org/10.1109/83.709666

97. Singh RN, Gahrooee DR (1989) Application of rock mass weakening coefficient for stability assessmenet of slopes in heavily jointed rock masses. Int J Surf Min Reclamamtion Environ.; 3(4):207–19. https://doi.org/10.1080/09208118908944277

98. Singh V, Rao SM (2005) Application of image processing and radial basis neural network techniques for ore sorting and ore classification, Mineral Engineering, 18(15) 1412–1420.

99. Sousa LMO, Gonçalves BMM (2012). Color assessment of granitic rocks and implications for their ornamental utilization. Color Research & Application, 37, 375–383. https://doi.org/10.1002/col.20681

100. Tating F, Hack R, Jetten V (2013) Engineering aspects and time effects of rapid deterioration of sandstone in the tropical environment of Sabah, Malaysia. Engineering Geology, 159, 20–30. https://doi.org/10.1016/j.enggeo.2013.03.009

101. Taylor SR, McClennan SM (1985) The Continental Crust: Its Composition and Evolution. Blackwell Scientific, Oxford.

102. Tembely M, AlSumaiti AM, Alameri WS (2021) Machine and deep learning for estimating the permeability of complex carbonate rock from X-ray micro-computed tomography. Energy Reports, 7, 1460-1472. https://doi.org/10.1016/j.egyr.2021.02.065

103. Terzaghi K, Peck R (1967) Soil mechanics in engineering practice. Wiley, New York

104. Thuro K (1997) Prediction of drillability in hard rock tunnelling by drilling and blasting. Proceedings of World Tunnel Congress, Vienna.

105. Thuro K, Spaun G (1996) Introducing the 'detruction work' as a to new rock property of toughness refering to drillability in conventional drill and blast tunnelling. Proceedings of International Society for Rock Mechanics and Rock Engineering (ISRM) International Symposium-Eurock'96, Turin.

106. Torabi-Kaveh M, Rizi FS, Tajbakhsh G, Khodami M, Ménendez B (2023) The use of chemical and textural indices to predict geotechnical properties of granites with different degrees of weathering. Bulletin of Engineering Geology and the Environment 82(9):362. https://doi.org/10.1007/s10064-023-03387-x

107. Toś C (2016) The use of a modified camera for the classification of sedimentary rocks. Photogrammetrie–Fernerkundung–Geoinformation, 4, 191–210. https://doi.org/10.1127/pfg/2016/0299

108. Tuğrul A, Zarif IH (2000) Engineering aspects of limestone weathering in Istanbul, Turkey. Bulletin of Engineering Geology and the Environment (58):191-206. https://doi.org/10.1007/s100640050075

109. Tuncdemir H, Bilgin N, Copur H, Balci C (2008) Control of rock cutting efficiency by muck size. International Journal of Rock Mechanics and Mining Sciences, 45(2), 278-288.

110. Turkington VA, Paradise TR (2005) Sandstone weathering: a century of research and innovation. Geomorphology 67(1-2):229-253. https://doi.org/10.1016/j.geomorph.2004.09.028

111. Ündül O, Tuğrul A (2012) The influence of weathering on the engineering properties of dunites. Rock Mech Rock Eng (45):225-239. https://doi.org/10.1007/s00603-011-0174-1

112. Xie WQ, Zhang XP, Liu QS, Tang SH, Li WW (2021) Experimental investigation of rock strength using indentation test and point load test. International Journal of Rock Mechanics and Mining Sciences, 139, 104647. https://doi.org/10.1016/j.ijrmms.2021.104647

113. Xie WQ, Zhang XP, Yang XM, Liu QS, Tang SH, Tu XB (2020) 3D size and shape characterization of natural sand particles using 2D image analysis. Engineering Geology, 279, 105915.

114. van Eldert J, Schunnesson H, Johansson D, Saiang D (2020) Application of measurement while drilling technology to predict rock mass quality and rock support for tunnelling. Rock Mechanics and Rock Engineering, 53(3), 1349-1358. https://doi.org/10.1007/s00603-019-01979-2

115. Yaralı O, Kahraman S (2011) The drillability assessment of rocks using the different brittleness values. Tunneling Undergr Space Technol.; 26(2):406–14 https://doi.org/10.1016/j.tust.2010.11.013

116. Yusoff IN, Ismail MAM, Tobe H, Miyoshi T, Date K, Yokota Y (2021) Weathered rock and crack detection of tunnel excavation using image analysis. In The Evolution of Geotech-25 Years of Innovation (pp. 475-483). CRC Press.

117. Weinert HH (1965) Climatic factors affecting the weathering of igneous rocks. Agricultural Meteorology 2(1):27-42. https://doi.org/10.1016/0002-1571(65)90033-6

118. Wu Z, Wei R, Chu Z, Liu Q (2021) Real-time rock mass condition prediction with TBM tunneling big data using a novel rock–machine mutual feedback perception method. Journal of Rock Mechanics and Geotechnical Engineering, 13(6), 1311-1325. https://doi.org/10.1016/j.jrmge.2021.07.012

119. Zhang Q, Liu Z, Tan J (2019) Prediction of geological conditions for a tunnel boring machine using big operational data. Automation in construction, 100, 73-83. https://doi.org/10.1016/j.autcon.2018.12.022

120. Zhang XP, Xie WQ, Cai KY, Liu QS, Wu J, Li WW (2021) Evaluation of rock muck using image analysis and its application in the TBM tunneling. Tunnelling and Underground Space Technology, 113, 103974.

121. Zhao J, Broms BB, Zhou Y, Choa V (1994) A study of the weathering of the Bukit Timah Granite. Part A: review, field observations and geophysical survey. Bull Eng Geol Environ (49):97-106. https://doi.org/10.1007/BF02595006

122. Zhao TB, Guo WY, Tan YL, Lu CP, Wang CW (2018) Case histories of rock bursts under complicated geological conditions. Bulletin of engineering geology and the environment, 77(4), 1529-1545. https://doi.org/10.1007/s10064-017-1014-7

123. Zhao J, Pan J, Hu Y, Li J, Yan B, Li C, Liu X (2021) Digital rock physics-based studies on effect of pore types on elastic properties of carbonate reservoir Part 1: Imaging processing and elastic modelling. Chinese Journal of Geophysics, 64(2), 656-669. doi: 10.6038/cjg2021O0228

124. Zhu X (1985) View of soft rock roadway support. Coal Sci Technol 8:21–23.

125. Zhu Y, Duan G, Chen B, Peng X, Chen Z, Sun G (2014) Mineral weathering and element cycling in soil-microorganism-plant system. Sci China Earth Sci 57:888–896. https://doi.org/10.1007/s11430-014-4861-0

126. Zhu H, Huang M, Ji P, Xiao F, Zhang QB (2025) Transforming the maintenance of underground infrastructure through Digital Twins: State of the art and outlook. Tunnelling and Underground Space Technology, 161, 106508.

127. URL 1 (2025) Image Color Summarizer 0.76 © 2006-2020 Martin Krzywinski mkweb.bcgsc.ca, (https://mk.bcgsc.ca/colorsummarizer/?analyze), accessed on September 2025.